EVALUATING THE RELATIONSHIP BETWEEN SOLAR CYCLE AND THE OCCURRENCE OF EL NIÑO-SOUTHERN OSCILLATION

By

TSION LEMA AYENACHWE

IN PARTIAL FULFILMENT OF THE REQUIREMENT FOR THE DEGREE OF MASTER OF SCIENCE IN EARTH SYSTEM PHYSICS (SPACE SCIENCE AND ASTRONOMY), INSTITUTE OF GEOPHYSICS SPACE SCIENCE AND ASTRONOMY, ADDIS ABABA UNIVERSITY

June, 2024

Addis Ababa, Ethiopia

EVALUATING THE RELATIONSHIP BETWEEN SOLAR CYCLE AND THE OCCURRENCE OF EL NIÑO-SOUTHERN OSCILLATION

By

TSION LEMA AYENACHWE

MAIN-ADVISOR: Dr. ELIAS LEWI

CO-ADVISOR: Dr. MOGESE WASSAIE

A THESIS SUBMITTED TO DEPARTEMENT OF SPACE SCIENCE AND ASTRONOMY, INSTITUTE OF GEOPHYSICS SPACE SCIENCE AND ASTRONOMY, ADDIS ABABA UNIVERSITY

IN PARTIAL FULFILMENT OF THE REQUIREMENT FOR THE DEGREE OF MASTER OF SCIENCE IN EARTH SYSTEM PHYSICS (SPACE SCIENCE AND ASTRONOMY)

June, 2024

Addis Ababa, Ethiopia

ADDIS ABABA UNIVERSITY

INSTITUTE OF GEOPHYSICS SPACE SCIENCE AND ASTRONOMY

DEPARTMENT OF SPACE SCIENCE AND ASTRONOMY

EXAMINERS' THESIS SUBMISSION APPROVAL SHEET

This is to certify that the thesis entitled "EVALUATING THE RELATIONSHIP BETWEEN SOLAR CYCLE AND THE OCCURRENCE OF EL NIÑO-SOUTHERN OSCILLATION" has been developed by Tsion Lema Ayenachwe (ID No GSR/8012/15), under our examination. Thus, we approved that the student submit their thesis for defense and evaluation.

Dr. Berhanu Abera	_____	_____
Chair- Person	Signature	Date
Dr. Kassahun Ture	_____	_____
External Examiner	Signature	Date
Dr. Abbi Seyoum	_____	_____
Internal Examiner	Signature	Date

Declaration

I certify that this Research Thesis is my work and to the best of my knowledge it has not been submitted or published elsewhere for examination, award of degree, or publication. Where other people's work or my work has been used, this has properly been acknowledged and referenced by the University of Addis Ababa requirements.

Student Name: Tsion Lema Ayenachwe Signature _____ Date: _____

Department/Unit: Space Science and Astronomy

College/Institute: Institute of Geophysics, Space Science and Astronomy (IGSSA)

This MSc Research Thesis is submitted for examination with our approval as research supervisors:

	Signature	Date
Name of Main advisor: Dr. Elias Lewi	_____	_____
Name of Co-advisor: Dr. Mogese Wassaie	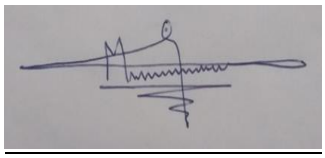	24/07/2024

Table of Contents

List of Figure

Acronym

- AP: Ap index (it is a planetary index that indicates the level of geomagnetic activity on a given day)
- CMEs: Coronal Mass Ejection
- Dst: Disturbance Storm Time
- ENSO: El Niño–Southern Oscillation
- FFT: Fast Fourier Transform
- IPO: Interdecadal Pacific Oscillation
- JMA: Japan Metrology Agency
- KP: Kennziffer (means index in Germany) planetary
- NOAA: National Oceanic and Atmospheric Administration
- ONI: Oceanic Nino Index
- SSC: Storm Sudden Commencement (SSC)
- SOI: Southern Oscillation Index
- SST: Sea Surface Temperature

Acknowledgment

First of all, I would love to thank the Almighty God. I also want to thank Addis Ababa University for awarding me women scholarship. Next, I would like to express my heartfelt gratitude to my advisors, Dr. Elias Lewi and Dr. Moges Wassie for their advice, encouragement, guidance, valuable criticism, and support in completing this thesis. Then, I would like to thank all the IGSSA members and my friends who supported and encouraged me while doing my thesis. Also, my sincere gratitude goes out to my entire family for their help, consideration, and encouragement while I worked on my thesis. In closing, I would like to express my gratitude to everyone who has given their valuable time to make this work successful.

Abstract

Quasi-periodic climate patterns like El Niño and La Niña exert significant impact on global weather patterns. As the primary source of energy for the Earth's climate system, changes in solar activity, including the 11-year solar cycle, have been hypothesized to influence the complex ocean-atmosphere interactions that govern ENSO dynamics. Despite extensive research efforts, a universally accepted theory elucidating the causes of these phenomena remains unclear. However, recent discoveries hint at a potential link between this quasi-periodic event and the solar cycle, sparking ongoing debate among researchers worldwide. In an effort to furnish additional context to this finding, we have conducted an analysis utilizing monthly average sunspot count data spanning from 1964 to August 2023, in conjunction with the Oceanic Niño Index of 3.4, from the same period. The data sets are first de-trended to remove any linear trend and filtered to remove possible noise in the high frequency spectrum. Then both data sets are transformed into the frequency domain. The amplitude spectrums of the two data sets are then analyzed and the coherency between them is explored to find if there is any relationship between the two data sets in the different frequency spectrums. Furthermore, the phase lag is analyzed, to see if there is discernable lag between the two data sets. The result revealed a statistically significant, high degree of coherency between sunspot activity, and the occurrence of El Niño events within certain frequency ranges. Specifically, the results showed a coherency at the 99% confidence threshold level, mainly with a periodicity of approximately 11.59 and 5.2 years, corresponding to the well-established 11-year and half the period of the solar cycle respectively. Taking into consideration the resolution capacity of the data, the analysis also reveals a monthly lag between changes in sunspots and the occurrence of ENSO events. Finally, the findings suggest that sunspot activity and El Niño events are not independent, isolated phenomena, but rather exhibit a meaningful, interconnected relationship. Numerous fields will benefit from this outcome, particularly the agricultural and climate forecasting sectors.

CHAPTER 1

1. INTRODUCTION

1.1. Background of the study

The Sun is one of the stars, and sunspot numbers are a well-known characteristic referred to as indices of solar activity (Lefèvre & Clette, 2011; Stix, 1981). Sunspot number is one of the measurable quantities to define solar activities and can also be associated with the strength of the Sun's magnetic field (Bravo et al., 1998; Hathaway, 2015; Mordvinov et al., 2016). A strong magnetic field causes sunspots to cool down to a lower temperature (about 4000 K as compared to 5800 K in the photosphere). These mean that they seem darker on the surface of the Sun's photosphere (Usoskin, 2017).

The solar activity has an average period of about 11 years, commonly referred to as a phase of the solar cycle. It is also sometimes called the Schwabe cycle or solar magnetic activity cycle (Hathaway & Wilson, 2004; Svalgaard et al., 2017; Usoskin & Mursula, 2003) and it is the most noticeable aspect of solar activity. During high solar cycles, it dominates sunspot activity for nearly the entire recorded time span. This cycle fluctuates on several time scales in terms of amplitude, period (duration), and shape (Usoskin, 2017).

El Niño, which means "the boy Christ-child" in Spanish, is one of the most well-known climate phenomena. It was initially used to describe an annual weak, warm ocean circulation that sweeps southward along the coast of Peru and Ecuador around Christmas (Philander, 1998). Only later did the term "El Niño" come to refer to the exceptionally large warmings' of Earth's atmosphere that happen every few years and alter the local and regional ecology. The opposite "La Niña" (or "the girl" in Spanish) phase is the cold phase of El Niño Southern Oscillation (ENSO). This is caused by a tropical Pacific basin-wide cooling. To the general public, the entire occurrence is referred to as "ENSO" (Trenberth, 1997).

Previous research has explored potential connections between El Niño-Southern Oscillation (ENSO) events and solar activity, as measured by sunspot numbers. According to Kunjaya et al. (2001) calculated the correlation between ENSO and sunspot data, concluding that these two phenomena do not exist in complete isolation from one another. Furthermore, Mumtahana et al. (2015) utilized Weighted Wavelet Z-Transform (WWZ) analysis to examine the relationship between ENSO and solar activity in both the frequency and time domains. Their analysis revealed a significant correlation between the two variables at periodicities of roughly 4-6 years.

While these previous studies have demonstrated a relationship between ENSO and solar activity, they have not conclusively determined the underlying mechanisms or time lags responsible for this connection. Kunjaya et al. (2001) studies claim that there is a correlation between the two events whereas Mumtahana et al. (2015) studies noted the presence of a 4-6 year periodicity in the correlation between the two phenomena, but did not quantify the phase lag or time delay between solar activity changes and the onset of ENSO events. In addition both the Kunjaya et al. (2001) and Mumtahana et al. (2015) studies does not show the ENSO activity with the phases of solar cycle.

Building on the previous research, the current study aims to provide a more detailed examination of the relationship between solar activity and the El Niño Southern Oscillation. Specifically, this work calculates the phase lag between solar activity and the onset of ENSO events. Despite the monthly resolution of the data, the analysis is able to quantify the time delay between solar cycle variations and the corresponding ENSO activity. Furthermore, the study explores the patterns and phases of ENSO occurrences in the context of the broader 11-year solar cycle. By analyzing how ENSO activity, including both El Niño and La Niña events, aligns with the different stages of the solar cycle, the study provides insights into the potential mechanisms linking solar variability to changes in tropical Pacific ocean-atmosphere dynamics.

1.2. Statement of the Problem

The Sun is the ultimate source of energy for our planet Earth. For instance, the solar activities can affect the Earth’s eco-system in many ways. In other words, the Earth's entire system can be

impacted by events on the Sun. One of the terrestrial events that are thought to be impacted by solar activities is ENSO. As has been studied by, e.g., Mumtahana et al., (2015), the solar cycle and ENSO are correlated. ENSO is an event in the Pacific Ocean, and there is no regular period for the events, but it generally occurs every two to seven years (McPhaden, 2002). It is the primary worldwide driver of the global climate change. The Sun is one of the numerous elements that are thought to be the cause of ENSO, while the exact explanation is still unknown and needs further research. Even though scientists examine the relationship between ENSO and solar activities, the issue is still hot and debatable.

Some scientists and researchers attempt to determine their association, using sunspot and ENSO index data (Kunjaya et al., 2001; Mumtahana et al., 2015; Zhai, 2017; Zhou et al., 2013). Some of them, for example, use the WWZ-transform tool to obtain similarities within a 4-6 year period. Furthermore, the WWZ-transform tool is used to attempt to determine the correlation between sunspot number and ENSO (Mumtahana et al., 2015). In this study, we investigate the correlation between the two signals in the frequency domain using the coherency method.

It is obvious that most global climatic conditions, including the Ethiopian rainfall pattern, are affected by ENSO (e.g., Diro et al., 2011; Eltahir, 1996; Enfield, 1989; Williams & Kniveton, 2011; Wolde-Georgis, 1997). However, it is not yet much investigated what causes ENSO with regard to space and time. For instance, better understanding and studying the relationship between the solar cycle and ENSO conditions can lay the foundation for the study of the possible causes of ENSO with regard to space and time.

1.3. Research question/Hypothesis

- Is the occurrence of ENSO affected by the Sun's activity?

- When does the solar cycle affect the ENSO condition?

- At which time does the solar cycle affect the ENSO condition significantly?

- What will be the time lag between the solar cycle and ENSO conditions?

1.4. Objectives of the Study

This thesis aims to investigate the relationship between ENSO and the phase of high solar activity in different solar cycles. The relationship between them is investigated by a technique/ tool of coherency analysis with standard fine lag time.

1.4.1. General Objective

The general objective of this research is to investigate the possible correlation between the occurrences of the Solar Cycle and ENSO.

1.4.2. Specific Objective

To meet the general objective, the following detailed objectives are set:

- Transform the data into the frequency domain and analyze and compare the amplitude spectra of both transformed signal.

- Evaluate the correlation of the two signals in the frequency domain and determine the specific frequency ranges where coherency occurs.

- Identify and assess any phase lag between the two signals

1.5. Significance of the study

The results of these studies will be advantageous in various sectors. Understanding how the solar cycle affects El Niño and La Niña and in which frequency range will mainly benefit the field of climate forecasting (Seleshi et al., 1994). Once their association is established, it will be

a crucial factor for forecasting ENSO events or forecast climatic extremes before they occur. As the proper knowledge of regions that can be impacted by a major ENSO allows us to take preventative measures that shield lives from natural hazards or take preventative action before the events harm humans and other living things (Hammer et al., 2000; L'Heureux et al., 2020; Weiher, 2000). Understanding their cause will strengthen the effort to reduce disaster or risk. It will also assist the livestock industry in changing and developing new and important strategies. In other words, this will lay the foundation for the development of new and improved forecasting techniques for ENSO conditions.

1.6. Scope of the study

This research was conducted to investigate the influence of the solar cycle on ENSO. To investigate their relationship, 59 years of data sets on the solar cycle and the ONI index are taken. Furthermore, the analysis is done in the frequency domain, to investigate the dominant periods/times in which they are correlated. Even though the data resolution doesn't fully allow carrying out the phase lag within days, it has been tested just to get a general picture about the phase lag if it is above the resolution capability of the data.

In this study, we are using only one well-known physical parameter from each event, i.e., the sunspot count and ONI index. Several other physical parameters of climate and solar variability are not included in this study.

1.7. Limitations of the study

Due to the availability of limited time, several other physical parameters of climate variability and solar events are not included in this study. Parameters related to solar variability, such as solar irradiance, different indexes, and cosmic rays, are not investigated. In addition, parameters related to climate variability, such as pressure, wind, humidity, and precipitation, are not taken into account.

The sunspot count and ENSO index are the only data sets used to investigate the coherency between the two events. It is however, known that the coherency analysis's output will only show that there is a correlation between two signals and it does not indicate the cause and effect relation between the two signals. This indicates that it is unclear about which event is the cause for the other one. In addition, the ONI data has a resolution of 1 month, and the phase lag analysis obtained will be indicative, not real.

To effectively utilize the output of this study for forecasting ENSO events, it is crucial to address and eliminate these limitations. This ensures that the findings of this study will be applied accurately and beneficially in forecasting ENSO phenomena.

1.8. Structure of the thesis

The second chapter analyzes the literature review on the properties of the solar cycle and ENSO and their relationship. Chapter 3 also deals with the data sets, the uses of scientific methods, and their processing using the Python language. Chapter 4 deals with the analyses, which are the result/outcomes and the discussion of the result. Finally, in Chapter 5, the conclusion of the research outcome is given, and recommendations are made.

CHAPTER 2

2. LITERATURE REVIEW

2.1. Solar activity

Just looking at the Sun through foggy skies, prehistoric humans noticed sunspots (Hathaway, 2015). These are dark patches on the Sun where strong magnetic fields loop up through the surface from the deep interior. When telescopes were first employed to examine the Sun in the early 17th century, they were surprised to see that the Sun has spots. The surprise came from the fact that the Sun and the skies were flawless and faultless (Hathaway, 2015).

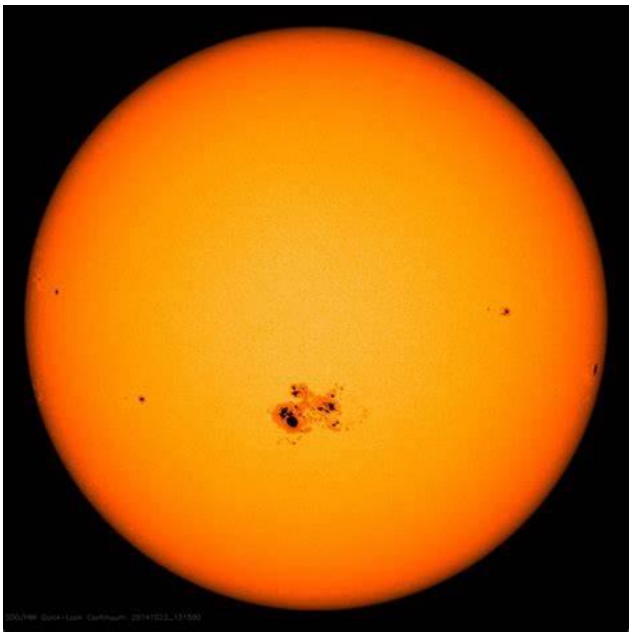

Figure 1: View of the sun with dark spots. Where the dark spot represents temporary, and they are cooler/reduced surface temperatures caused by concentrations of magnetic flux that inhibit convection. Sunspots appear within active regions, usually in pairs of opposite magnetic polarity (Credit to: https://th.bing.com/th/id/OIP.O4pJ0YvAnEMrB1fNutqAtQHaHa?rs=1&pid=ImgDetMain)

Some numerical measures that are related to the entire condition of the Sun (or a large portion of it) are essential, to analyze the statistical properties of solar activity (Stix, 1981). These characteristics are referred to as solar activity indices. Nowadays, numerous indices can indicate the strength of solar activity, for instance, the electromagnetic radiation different bands such as 10.7 cm radio flux, green corona, faculae, flares, and coronal holes. But the most well-known and frequently utilized index is sunspot activity, or the quantity of sunspots on the solar disk. It represents the fluctuating strength of the hydro-magnetic dynamo process, which creates the solar magnetic field.

The longest continuous series of solar measurements serves as its foundation. Soon after the invention of the telescope in 1610, Galileo started making regular observations of sunspots. Regular observations have been made ever since for nearly four centuries. The sunspot number is perhaps the most studied time series in astronomy and the most commonly used indicator of solar activity.

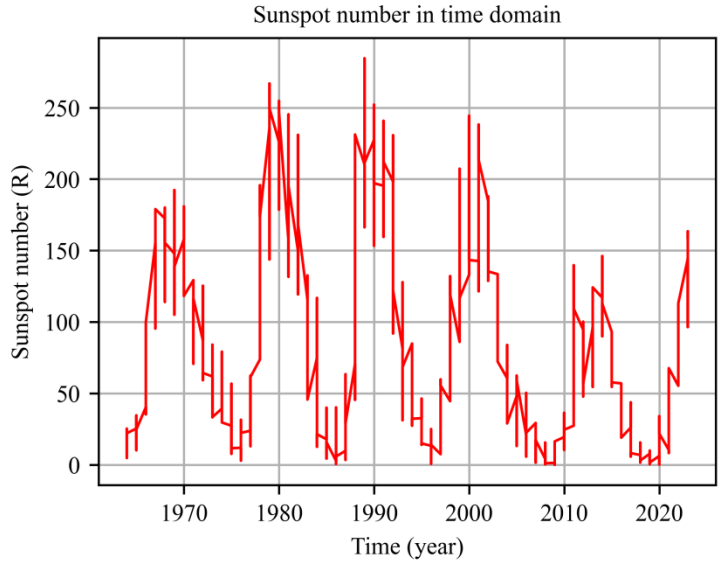

Figure 2: The Solar cycle of the sun observed from 1964 to 2023

The sunspot cycle was not formally identified until the year 1844, although Christian Horrebow refers to this potential periodic variation in the year 1776. Heinrich Schwab reported on his

study of the sunspot cycle in the year of 1844. Using data spanning 18 years, from 1826 to 1843, he came to the conclusion that the cycle lasted roughly 10 years (Hathaway, 2015).

Schwabe's finding on the sunspot cycle most likely played a major role in starting the Johann Rudolf Wolf's (first at the Bern Observatory and then at Zurich) to gather daily observations of the Sun's data and extend the records backward in time (Hathaway, 2015).

A wide range of studies used common indices such as AP, KP, and Dst to gauge differences in the long-term progression of solar activity is the sunspot relative number, often known as the Wolf number. It was created in 1850 by the Swiss astronomer Johann Rudolf Wolf (Friedli, 2020). The amount that indicates how much of the solar surface is covered in dark spots is known as the Sunspot Number, or Wolf Number (R) (Hathaway, 2015; Hathaway & Wilson, 2004; Lomb, 2013). This can also be a reliable indicator of solar activity. The Sunspot Number varies periodically over (about) eleven years, reflecting the periodicity of solar activity. This phenomenon is known as the Solar Cycle (Kunjaya et al., 2001). According to Friedli, (2020) and Hathaway & Wilson, (2004), every day its value [R] is ascertained as:

$$R = K(10g + f) \qquad (1)$$

Where k is a personal reduction factor that converts the observed Wolf numbers from their raw instrumental system to a common standard system, g is the total number of sunspot groups as visible on the solar disk and f is the number of individual spots within the groups.

Dark areas on the Sun's surface are known as sunspots. It indicates the entire Sun's activity. In general, solar activity can be measured by the sunspot. A sunspot cycle is a roughly 11-year cycle that is periodic, it varies in the number of sunspots observed on the Sun's surface are used to assess variations in the Sun's activity.

A rise and fall in sunspot numbers and surface area is a characteristic of the 11-year solar activity cycle (Hathaway, 2015). A solar cycle can be distinguished from another by its intensity, period,

amplitude, and other characteristics. Furthermore, there is variation in the quantity of sunspots/black spots across the 11-year solar cycle, which can lead to either solar minimum or solar maximum.

2.2. El Niño Southern Oscillation

"El Niño" refers to the exceptionally large warmings' of Earth's atmosphere that happen every few years and alter the local and regional ecology. The opposite "La Niña" phase is the cold phase of El Niño Southern Oscillation (ENSO).

According to Philander, (1985), the two complementary phases of the southern oscillation are called El Niño and La Niña. The greater atmospheric release of latent heat causes instability during El Niño. Whereas during La Niña, the atmosphere cools down, convection compresses into progressively smaller regions, allowing for instability that amplifies the oceanic current and trade wind.

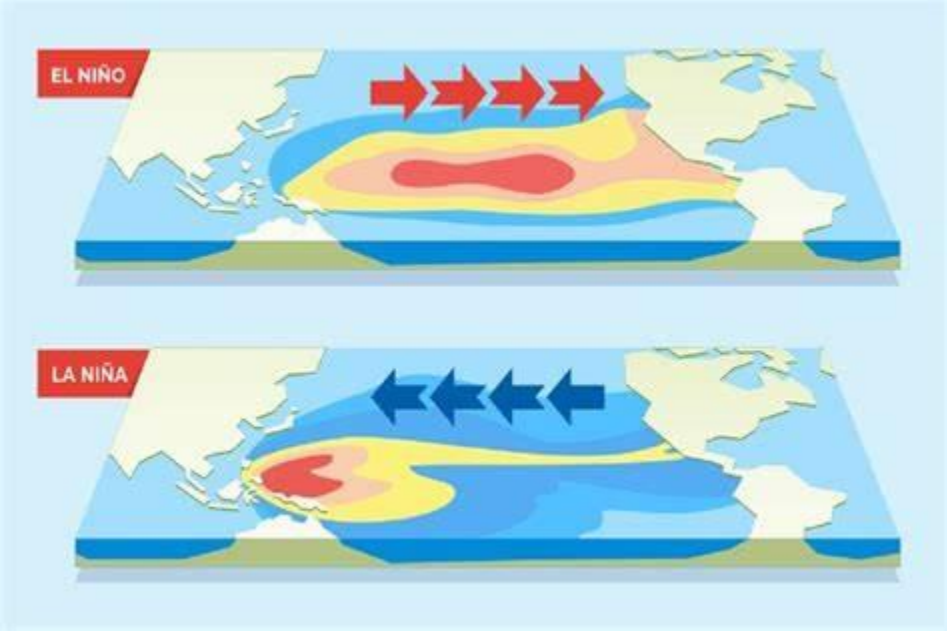

Figure 3: El Niño, La Niña and the trade wind. It's a simple picture of El Niño and La Niña with an arrow indicating the direction of the trade wind (Credit to: https://th.bing.com/th/id/OIP.xjlwVNKfYphDp7MU8s7xAAAAAA?rs=1&pid=ImgDetMain)

Within the tropical Pacific's connected ocean-atmosphere climate system, El Niño and its atmospheric counterpart, the Southern Oscillation, seem to arise as an internal cycle of positive and negative feedback (Enfield, 1989).

As Figure 3 illustrates during an El Niño event, the prevailing trade winds in the tropical Pacific Ocean reverse direction, blowing from the west to the east. Conversely, during a La Niña period, the trade winds revert to their normal easterly flow, moving from the east to the west direction across the equatorial Pacific.

2.3. The Solar Cycle and ENSO Condition

There are a number of factors that affect the Earth's climate for a long period of time. Some of the factors are energy coming from the Sun, change in the Earth's orbit, axial and precession, contents of greenhouse gases in the atmosphere, quantity of carbon dioxide in the Ocean, plate tectonic and volcanic eruption activities, change of land cover and the impact of Meteorites (Brovkin et al., 2004; Crowley, 2000; Gibbard et al., 2005; Lourens, 2021; Mikhaylov et al., 2020; Pielke Sr et al., 2011; Scafetta et al., 2020; Vérard et al., 2015).

From all those activities the energy that comes from the Sun related to the ENSO condition is studied here and it may have a positive relation with ENSO. The Sun is the source of almost all energy that influences Earth's climate. The energy from the Sun travels across space before entering the atmosphere of Earth. The Earth's surface receives only a portion of the solar energy that is intercepted at the top of the atmosphere; the remainder is absorbed by the atmosphere and reflected into space. Furthermore, because the Sun's energy production is not constant, it has an impact on our climate. We may observe, for instance, the differences in influence between the solar minimum and maximum phases of the cycle.

A roughly 11-year cyclical variation in solar activity, known as the solar cycle, is characterized by variations in solar radiation, solar flare frequency, and sunspot count. The magnetic dynamo activities that produce and intensify magnetic fields inside the Sun are what propel this cycle. These processes are caused by the solar plasma's differential spin. The terms "solar minimum" and "solar maximum" refer to the Sun's corresponding phases of increasing and decreasing activity during a solar cycle. Whereas solar minima show lower solar activity and fewer sunspots, solar maxima are distinguished by more sunspots and more solar irradiance. These fluctuations have a major influence on space weather, changing solar wind intensity and UV radiation, which in turn affects satellite operations, communication systems, and even Earth's climate (Hathaway, 2015).

The solar minimum is characterized by the conclusion of the previous solar cycle, the start of the next, and a decrease in solar activity (Harvey & White, 1999). The 11-year solar cycle's solar minimum is the time when solar activity is at its lowest. During solar minimum number of sunspots becomes low or there are no sunspots at all as a result the Sun becomes quiet/inactive relative to solar maximum. Throughout solar minimum, several events happen in the space weather and Earth’s atmosphere.

At solar minimum, streams are preferentially linked to weaker storms (Richardson et al., 2001). The Sun's magnetic field is less complicated and weaker during this period. The solar wind can more readily escape the Sun's gravitational attraction when there is less magnetic field strength in the Corona holes, the outermost region of the Sun (Lee et al., 2011). Fast solar wind streams that can occasionally result in mild to moderate geomagnetic storms originate from coronal holes. Consequently, at solar minimum, the solar wind is more likely to be powerful and persistent. The solar wind generally has higher particle densities and velocities.

The inverse relationship/anti-correlation between IMF and cosmic ray is shown by (Bieber et al., 1993; Cane et al., 1999). The interplanetary and solar magnetic fields were weaker during the solar cycle 23 minimum period than they were during earlier minimum periods (Lee et al., 2011). As stated above those occurrences indicate that during solar minimum, the Earth's magnetic field

becomes weaker and as a result, the amount of cosmic rays that penetrate the Earth's atmosphere increases.

The Earth's magnetic field tends to weaken during solar minimum due to the following reasons:

- Reduced solar activity: During solar minimum, the Sun's magnetic activity and energy output are at their lowest point in the 11-year solar cycle (Harvey & White, 1999). This reduced solar activity leads to a weaker interplanetary magnetic field, which interacts with and shapes the Earth's external magnetic field.

- Decreased solar wind pressure: The solar wind, which is driven by the Sun's magnetic activity, is less intense during solar minimum. The lower solar wind pressure allows the Earth's magnetosphere to expand, reducing the compression of the Earth's external magnetic field.

- Changes in the magnetosphere: With the decreased solar wind forcing, the Earth's magnetosphere becomes less distorted and compressed during solar minimum. This allows the Earth's intrinsic, dipole-like magnetic field to become more dominant, reducing the contributions from external currents (Lanza & Meloni, 2006).

- Variations in the geomagnetic dynamo: The generation of the Earth's internal magnetic field by the geodynamo in the liquid outer core is influenced by changes in the Sun's activity. During solar minimum, subtle variations in the geomagnetic dynamo can lead to a temporary decrease in the overall magnetic field strength (Courtillot et al., 2007).

- Increased cosmic ray influx: As mentioned earlier, the reduced magnetic field during solar minimum allows more cosmic rays to penetrate the atmosphere. This increased cosmic ray bombardment can potentially influence the geomagnetic dynamo and contribute to the overall decrease in the magnetic field strength (Hedgecock, 1975).

In summary, the combination of reduced solar activity, decreased solar wind pressure, changes in the magnetosphere, variations in the geomagnetic dynamo, and increased cosmic ray influx all contribute to the general weakening of the Earth's magnetic field during the solar minimum phase of the solar cycle.

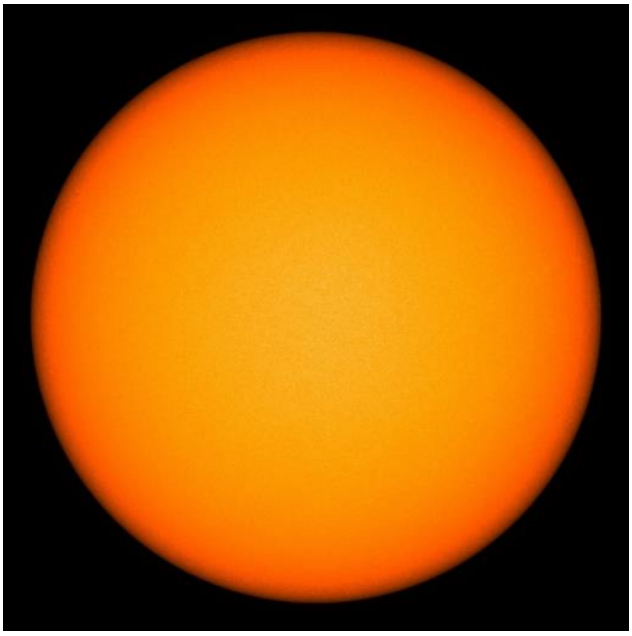

Figure 4 The outer surface of the Sun during solar minimum condition (Credit to: https://freestarcharts.com/images/Articles/Glossary/Solar_Min.jpg).

The Sun's 11-year solar cycle's solar maximum is the regular time of highest solar activity. It represents the peak of the 11-year cycle. It is the opposite of the solar minimum. The 11-year solar cycle's solar maximum is the time when solar activity is at its highest level. During solar maximum the number of sunspots becomes high as a result the Sun becomes active relative.

The Sun's magnetic field becomes more unstable and complicated during solar maximum. During solar maximum several events happen in the space weather and Earth’s atmosphere, which increases the frequency and intensity of solar flares, prominences, the incident of a storm

sudden commencement (SSC), and CMEs (Bocchialini et al., 2018). Large-scale plasma and magnetic field eruptions from the Sun's corona are known as CMEs. They may cause problems for electrical grids, satellite operations, and communication networks, as well as have a substantial effect on Earth's space environment.

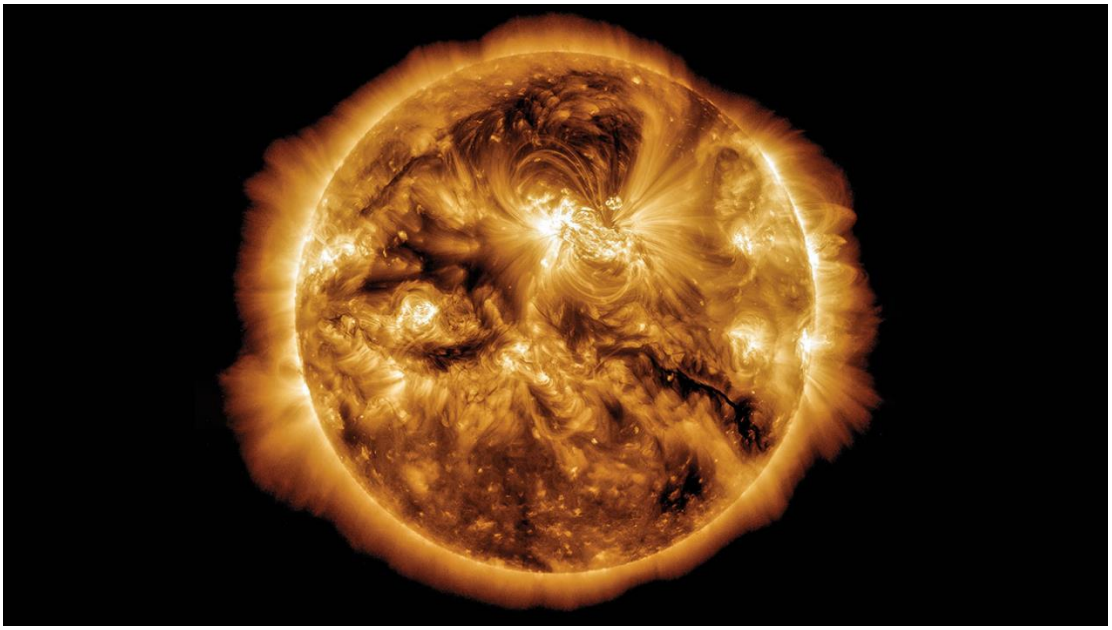

Figure 5: The outer surface of the Sun during Solar maximum (Credit to: https://vajiram-prod.s3.ap-south-1.amazonaws.com/What_is_the_Solar_Maximum_4c998371f0.jpg)

At solar maximum, the Earth's magnetic field becomes stronger for many main reasons:

- Increased solar activity: During solar maximum, the Sun's magnetic activity and energy output are at their highest point in the 11-year solar cycle. This increased solar activity leads to a stronger interplanetary magnetic field, which interacts with and compresses the Earth's external magnetic field.

- Increased solar wind pressure: The solar wind, driven by the Sun's magnetic activity, is more intense during solar maximum. The higher solar wind pressure compresses the Earth's magnetosphere; causing the internal magnetic field to become stronger.

- Changes in the magnetosphere: With the increased solar wind forcing, the Earth's magnetosphere becomes more compressed and distorted during solar maximum. This allows the Earth's internal, dipole-like magnetic field to become more dominant, as it is reinforced by the external currents in the magnetosphere.
- Variations in the geomagnetic dynamo: The generation of the Earth's internal magnetic field by the geodynamo in the liquid outer core can be influenced by changes in solar activity. During solar maximum, the subtle variations in the geodynamo can lead to a temporary increase in the overall magnetic field strength.

- Decreased cosmic ray influx: The stronger magnetic field during solar maximum shields the Earth more effectively from cosmic rays, reducing their influx into the atmosphere. This decreased cosmic ray bombardment can potentially contribute to the overall increase in the magnetic field strength (Hedgecock, 1975).

In summary, the key factors that lead to an increase in the Earth's magnetic field strength during solar maximum are the increased solar activity, higher solar wind pressure, changes in the magnetosphere, and variations in the geomagnetic dynamo, and the decreased cosmic ray influx. The Earth's internal magnetic field becomes more dominant during this phase of the solar cycle. Fluctuations in solar activity can influence global climate patterns, including the El Niño-Southern Oscillation (ENSO) phenomenon in the tropical Pacific.

El Niño and La Niña that form the Southern Oscillation are regarded as key phenomena in the Pacific that affect global weather conditions. In Spanish, “El Niño " (meaning "the little boy") then refers to the warm period of ENSO. The opposing “La Niña " phase, often known as "the little girl" in Spanish, is the cold phase of ENSO. This is caused by a tropical Pacific basin-wide cooling. But to the general public, the entire occurrence is referred to as “El Niño "(Philander, 1998). According to Glantz & Ramirez, (2020) and Kessler, (2002), El Niño is the phase of the ENSO quasi-periodic cycle in air-sea interactions in the tropical Pacific that is characterized by anomalously warm sea surface temperatures and the duration of the ENSO event varies from 5 to 27 months (Ray & Giese, 2012).

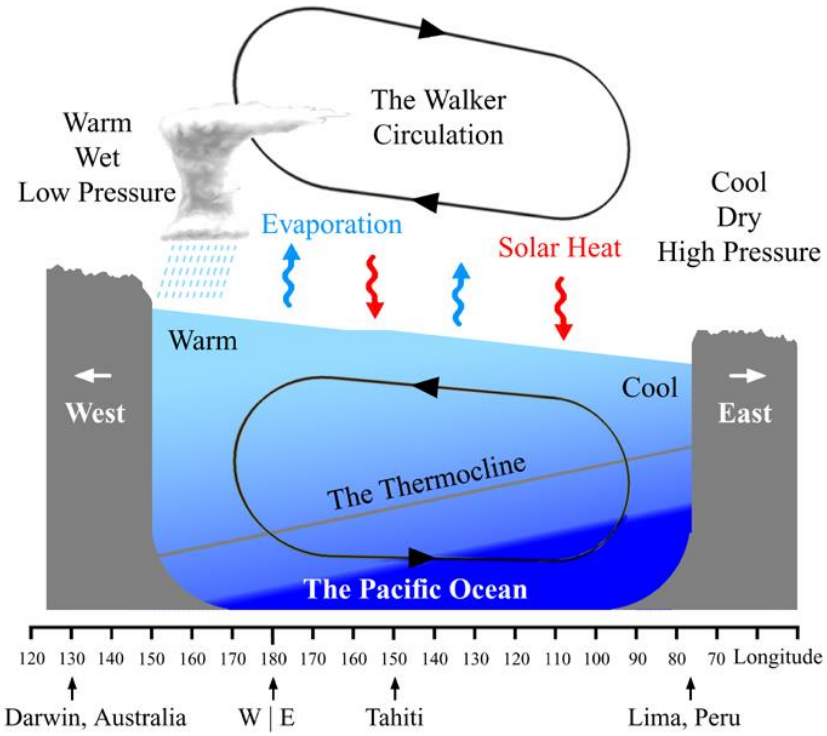

Figure 6: Ocean-atmosphere coupling shows the movement of water within the ocean. The West Pacific is warmer than the East Pacific. More clouds, rain, and low air pressure are caused by the warmer waters over the West Pacific. The accumulation of warm seas in the west also results in a thicker layer of warm ocean water, which decreases the thermocline's depth (Credit to: LaNina - El Niño–Southern Oscillation - Wikipedia).

El Niño- Southern Oscillation, which is associated with both atmospheric and oceanic anomalies and is an irregular or quasi-periodic phenomenon that occurs every two to seven years in the equatorial Pacific (Philander, 1985; Philander, 1998). This causes variance in the global climate system. It results in a protracted drought in one area and heavy precipitation in another (Eltahir, 1996; Wolde-Georgis, 1997). During the occurrence of El Niño its signature can last anywhere from nine to eighteen months. Using the Oceanic Nino Index (ONI) threshold criteria, 23 El Niño occurrences were officially recorded between 1950 and 2020 (Glantz & Ramirez, 2020). A climatic phenomenon known as the El Niño-Southern Oscillation alternates quasi-periodically between the neutral, La Niña, and El Niño phases.

- The Neutral phase: it's the suitable season. Its ONI represents between 0.5 and -0.5, if the condition lay between these two ranges, then the condition is neither El Niño nor La Nina. It does not cause any natural hazards. It's suitable for living things.

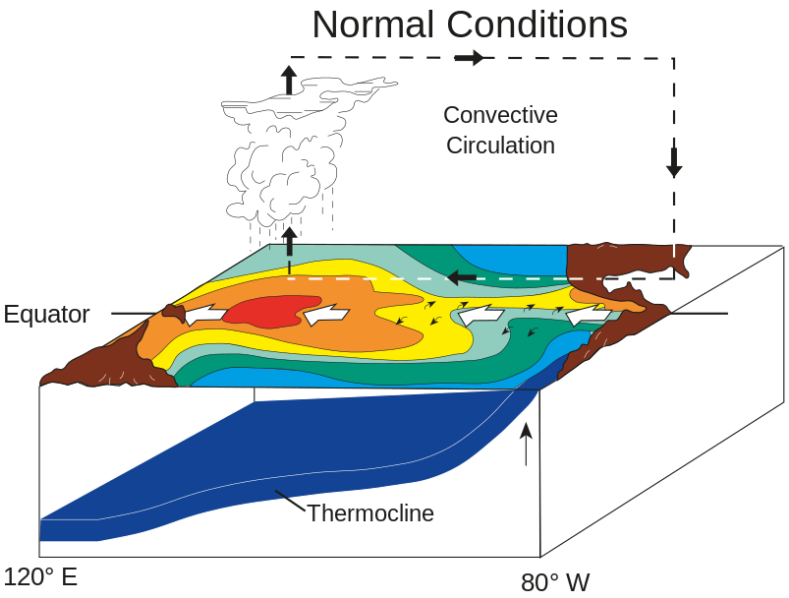

Figure 7: The Neutral phase/condition Warm water pools are gathered toward the west by equatorial winds. Deep atmospheric convection is driven by a warm pool toward the west (Credit to: https://upload.wikimedia.org/wikipedia/commons/thumb/b/b8/ENSO_-_normal.svg/800px-ENSO_-_normal.svg.png).

- El Niño phases: it is the hotter season of ENSO. During the warm phase of ENSO, the genesis frequency rises in the southeast and falls in the northwest of the western North Pacific (Kim et al., 2011).

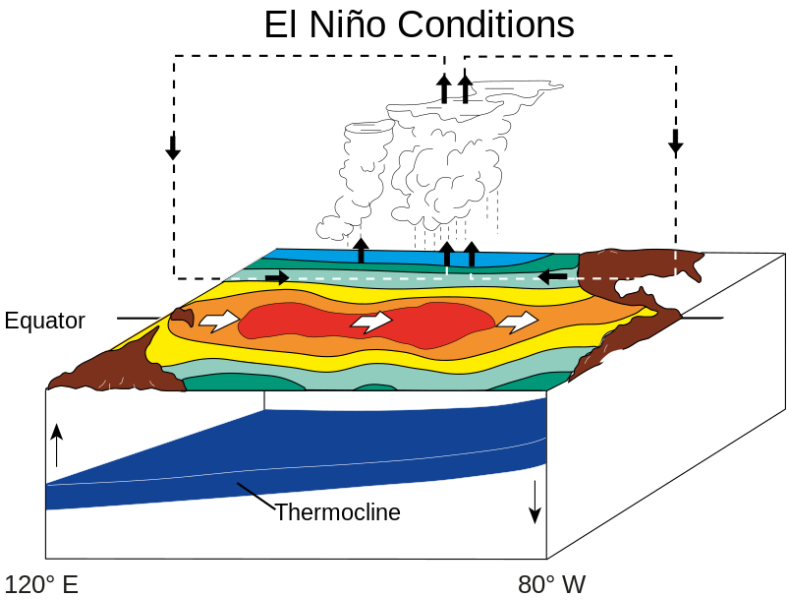

Figure 8: El Niño phases/ condition where the “Trade winds" reduce or reverse during El Niño occurrences, carrying warm surface waters eastward instead (Credit to: https://upload.wikimedia.org/wikipedia/commons/thumb/2/2f/ENSO_-_El_Ni%C3%B1o.svg/800px-ENSO_-_El_Ni%C3%B1o.svg.png).

La Niña phase: the cooler phase of ENSO is called La Niña, which is the opposite of El Niño. Wintertime temperatures in the North are usually colder than average during a La Niña year, whereas those in the South are generally warmer. La Niña can also lead to a more severe hurricane season (e.g., Klotzbach, 2011; Pielke Jr & Landsea, 1999).

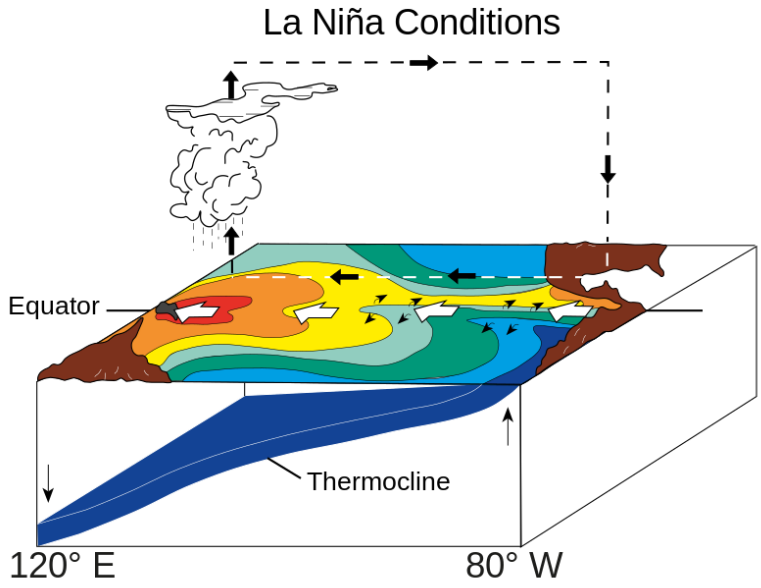

Figure 9: La Niña phase/conditions, represents the condition of La Niña phase. The normal east-to-west/"Trade winds" winds become stronger and push warmer waters further to the west. This results in cold water rising to the surface of the ocean, or "upwelling," from its depths, causing sea surface temperatures in the East Pacific to be lower than normal (Credit to: https://upload.wikimedia.org/wikipedia/commons/thumb/a/ab/ENSO_-_La_Ni%C3%B1a.svg/800px-ENSO_-_La_Ni%C3%B1a.svg.png).

The Sun is the major energy source of the Earth. Any activity on the Sun can affect the entire system of the Earth and its atmosphere. Activities on the Earth can be represented by using sunspot number. El Niño and La Niña significantly affect the Earth's climate and many scientists globally try to study the real cause of El Niño and La Niña (e.g., Glantz, 2001; Rodrigues & McPhaden, 2014; Su et al., 2010). Since the activity of the Sun affects the condition of the weather, some scientists study the relationship (impact or influence) of the solar cycle on El Niño and La Niña (Mumtahana et al., 2015; Radiman et al., 2009; Zhai, 2017).

Numerous countries have experienced natural disasters because of the El Niño and La Niña occurrences. Increases in the frequency and intensity of certain natural disasters, such as floods, droughts, and tropical cyclones, have been linked to the El Niño-Southern Oscillation; a recurring pattern of climate variability in the tropical Pacific marked by anomalies in air pressure and sea surface temperatures. Millions of people in many places have experienced numerous losses amounting to millions of dollars (e.g., Glantz, 2001; Grove & Adamson, 2018). However, precise cause of the ENSO phenomena is not yet known.

Since the Sun is the primary factor in determining the Earth's temperature, it makes sense to believe that variations in the Sun's activity could have an impact on Earth's climate, including the El Ninõ and La Niña phenomena (Kunjaya et al., 2001). The output of the solar energy package is represented by the total sunspot at each interval. Those envelopes containing total sunspot numbers are related to the ENSO phenomena (Mumtahana et al., 2015).

According to Kunjaya et al., (2001), El Niño and Sunspot cannot exist in complete isolation. ENSO may be intimately linked to the unique phase of maximum and minimum of the 11-year sunspot cycle and other solar cycles in terms of intense solar eruption, regardless of variations in Earth's rotation. Analysis of the data reveals that, at roughly 4-6 years, there is a similar period between those data (Mumtahana et al., 2015).

According to Stager et al., (2007), demonstrate that there is a connection between high rainfall and the solar cycle using more time domain techniques. Furthermore, the maximum solar cycle occurs 1-2 years after heavy rains. El Niño frequency and intensity are highest during secular solar minimum and lowest during secular solar maximum. In the 11-year solar cycle, El Niño reaches a statistically significant minimum roughly a year before the peak of solar activity (Kirov & Georgieva, 2002).

Furthermore, there is a paper that indicates there is a 60-Year Cycle in the Meteorite Fall Frequency Suggests a Possible Interplanetary Dust Forcing of the Earth's Climate Driven by

Planetary Oscillations (Scafetta et al., 2020). This influence may be one causes of ENSO event within a large time scale.

CHAPTER 3

3. DATASETS AND PROCESSING TECHNIQUES

To analyze the coherency between the Sunspot count and ONI data sets, the data sets are transformed to the frequency domain. Then the whole analysis of the data sets is done in the frequency domain. This is implemented using the Python programming language.

3.1. Data

We employ coherency technique/method to characterize/analyze the relationship between the Sunspot count and ONI, using datasets obtained from the Climate Prediction Center - ONI (noaa.gov). The SOI, Niño-3.4, and Niño-4 indices are more sensitive than the JMA and equally susceptible to El Niño events (Hanley et al., 2003).

The main tool used by NOAA to track the oceanic component of the seasonal El Niño-Southern Oscillation, or "ENSO," climatic pattern is the Oceanic Niño Index (ONI)/ Niño-3.4. Using NOAA's Oceanic Nino Index (ONI), sea surface temperatures (SSTs) in the central Pacific Ocean are tracked historically to determine the frequency and duration of El Niño occurrences (Glantz & Ramirez, 2020).

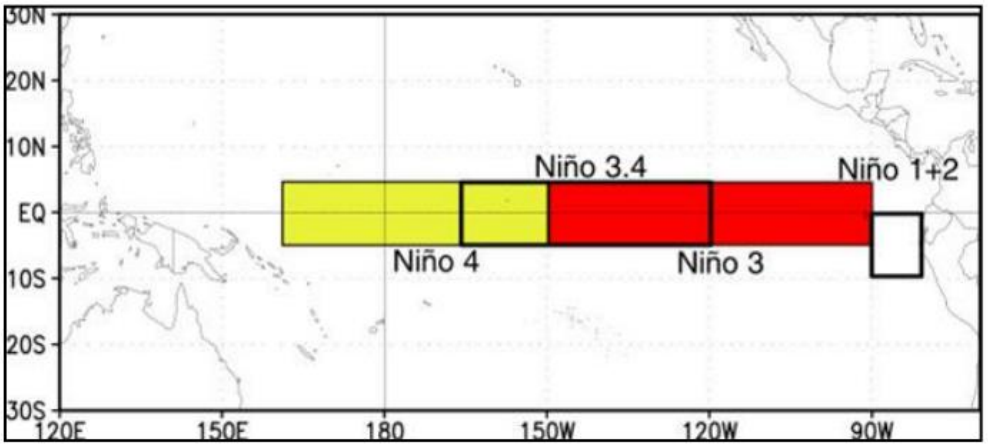

Figure 10: Area/region covered by Niño-3.4 (Credited to: https://upload.wikimedia.org/wikipedia/commons/2/2e/NinoRegions.png)

The Area/region covered by Niño-3.4 is indicated by the middle box, which is half yellow and half red box. As illustrated in figure 10 it represents 5N-5S, 170W-120W region of the Pacific Ocean. It also indicates the central part of the Pacific Ocean.

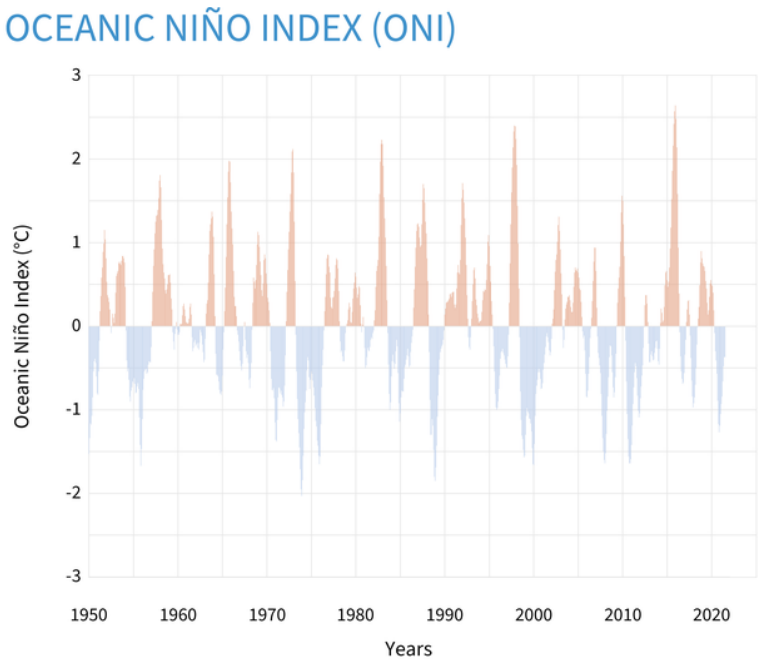

Figure 11: ENSO seasons based on ONI classification. The blue color denotes La Niña season and the red color indicates El Niño season. (Credit to: https://www.climate.gov/sites/default/files/styles/full_width_620_original_image/public/2021-09/ENSOblog_ONI_1950-present_20210923_2600.png?itok=sniXWFZO)

The historical occurrences of El Niño and La Niña are shown in Figure 11. Based on the ONI, an event is classified as La Niña if the ONI value is less than -0.5 and as El Niño season if the ONI value is larger than 0.5. Furthermore, based on the magnitude of the ONI value the strengths of the La Niña and El Niño event are categorized as weak, moderate, strong, and very strong.

Currently, the webpage that is widely used to obtain sunspot data is "OMNI (OMNIWeb Data Explorer (nasa.gov))" and it provides a multitude of parameters about phenomena occurring in the sun, for instance, Solar index F10.7, Lyman Alpha Solar Index, W/m^2 and so on. To study solar activity, it is better to choose the sunspot data number due to the length of data availability (Hathaway, 2015).

For our study, we have used the sunspot number data recorded from 1964 up to August 2023. These datasets are almost five phases of the solar cycle within 59 years. Thus, in this study all the available monthly data set during the common period starting from 1964 up to August 2023, has been used to investigate the correlation between them. Since there are five solar cycles within this range of 59 years, the data set is large enough to see if there is any relation between the two data sets.

3.2. Methodology

As Figure 12 illustrates the solar cycle data set is first plotted in the time domain to see the number of solar cycles during the specified period. In this range, there are five and a half (11/2) clear solar cycles. In the contrary, during this time range, as shown in Figure 22 of the appendix several El Niño events (the events may be strong, moderate, or weak) took place. These large ranges of data taken allow us to see their relation in the past and make a conclusion based on the output.

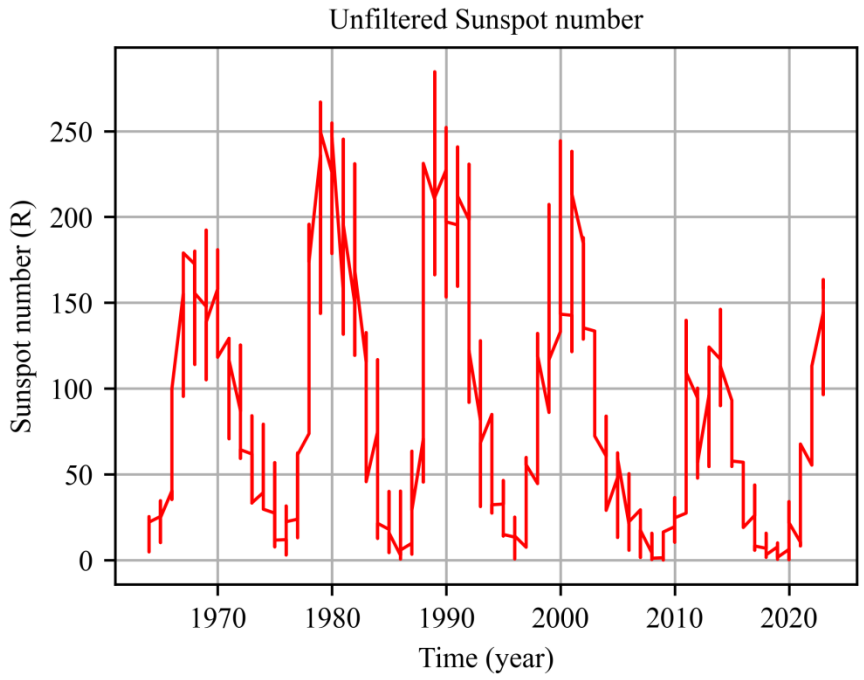

Figure 12: Solar cycle of the data in yearly time Series

3.2.1. Data filtering

As seasonal signals are the dominating amplitudes in the higher frequency ranges and because the target of this study is to analyze the correlation between the two data sets that are occurring in the longer wavelength spectrum, it was imperative to filter the high frequency signal to come up with a viable solution. Therefore, the first step in the data processing was the filtering of the high-frequency part of the signal. It is a widely accepted fact that data sets are filtered to improve processing efficiency, improve data quality, reduce data redundancy, and yield more accurate and better results, which in turn allows the evaluation of results in a better fashion. Removing errors and outliers (noises) from the data makes data interpretation easier.

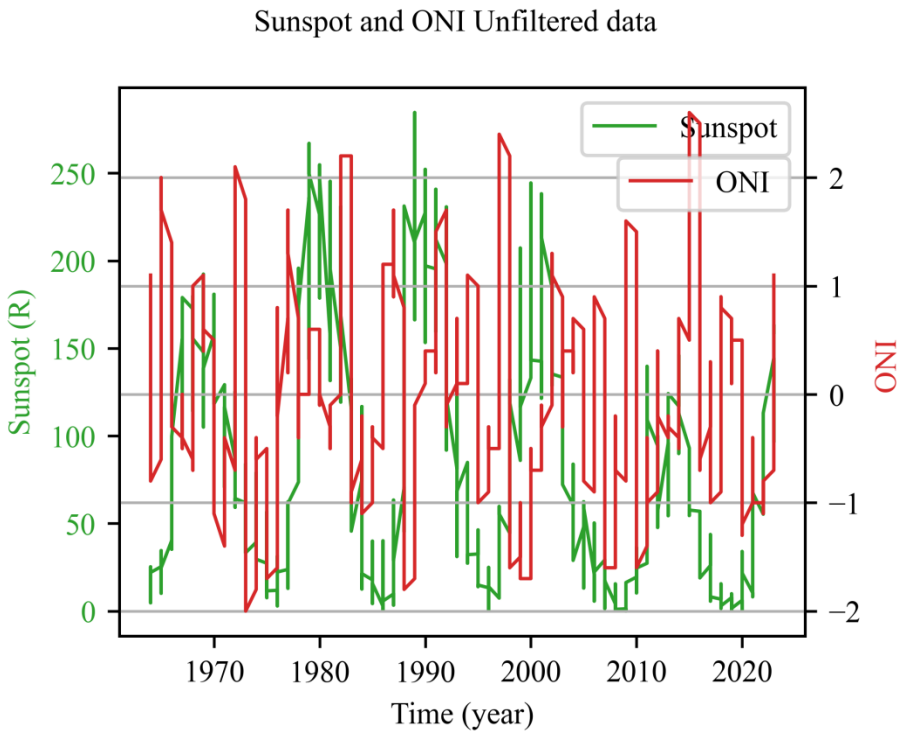

Figure 13: Sunspot and ONI unfiltered data versus time series from 1964 to 2023. It indicates that the monthly averaged sunspot (green: left y-axis) and the monthly averaged ONI index (orange: right y-axis), respectively.

Figure (13) is the plot of the Solar Cycle data before filtering. When plotting the data points, sharp spikes are observed in the graph, primarily caused by extremely large and small values. These outliers constitute noise, defined as random variations in the signal inherent to any data collection or measurement process. Failure to eliminate this noise can significantly affect the accurate interpretation of the signal. To address this issue, a digital filtering method is employed to mitigate these anomalies.

Various digital data filtering techniques play a crucial role in analyzing time series datasets. In this thesis, we implemented the widely recognized Savitzky-Golay (S-G) filtering technique. This filter is a member of the digital filters, which is instrumental in manipulating discrete-time signals by applying mathematical operations, thereby enabling adjustment of the signal spectrum as required (Hamming, 1998; Rader & Gold, 1967).

Filtering is a recognized method for removing irrelevant components from a signal and highlighting desired elements. In scientific research, digital filters are commonly employed to attenuate high-frequency noise and facilitate data smoothing (e.g., Juckett, 2010; Uzal et al., 2012). The Savitzky-Golay (S-G) filter, introduced by Savitzky and Golay in 1964, specifically aims to smooth noisy data by fitting a least squares polynomial over a moving window in the time domain (Savitzky & Golay, 1964). This method retrieves polynomial coefficients using linear matrix inversion before applying them in the filtering process (Press & Teukolsky, 1990; Schafer, 2011). Notably, S-G filters are very famous for their capacity in reducing noise levels while preserving essential data features such as peak height, width, and waveform structure (Guiñón et al., 2007; Schafer, 2011) making them preferable over alternative filtering techniques.

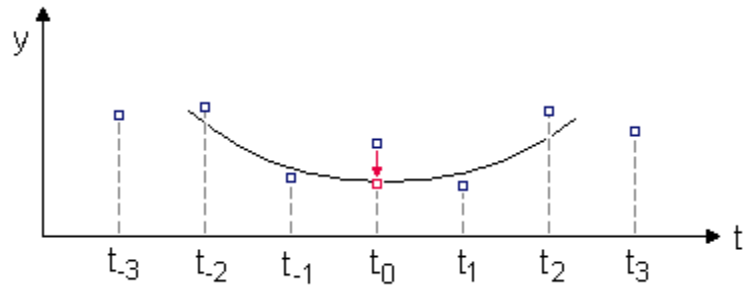

Figure 14: The Savitzky-Golay filter operation shown in a simple graph. The red square indicates the position at which we would like to compute the filtered data (Credit to: http://www.statistics4u.info/fundstat_eng/img/hl_savgol.png)

The polynomial fit at the center point determines the filter estimate at each window's center. In this method the window *w* is usually an odd integer to make the calculation easier (Gallagher, 2020).

In Figure 14 the S-G filter make use of a window size of five. Once the window size is decided the center of the window will be located at the point whose filtered counterpart is to be calculated. Since we use an odd number to simplify the calculation, it is simpler to identify the data center in the window as its size increases. However, the new projected value will be placed at the center. The shape of the filter is to be decided by the degree of the polynomial. Moreover, weighted least squares can be employed to exert greater control within S-G filters (Gallagher, 2020).

In this study, a window size of 25 was chosen to effectively mitigate high-frequency variations with wavelengths shorter than 24 months. This deliberate choice aims to eliminate seasonal fluctuations unrelated to ENSO or the solar cycle, thereby enhancing the prominence of ENSO and Solar Cycle amplitudes. Figure 15 and Figure 23 accessible in appendix illustrates the effectiveness of the Savitzky-Golay (S-G) filter in smoothing Sunspot and ONI data respectively.

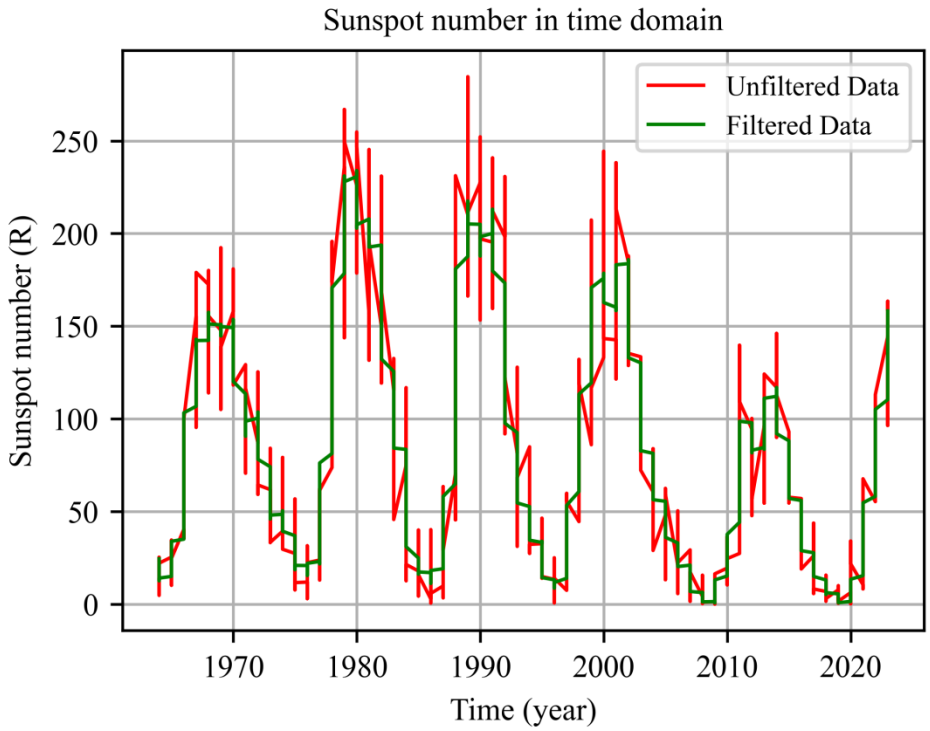

Figure 15: Filtered data of Sunspot, illustrates how the data's noise has been removed.

As it can be seen from Figure (15), the application of the Savitzky-Golay filter results in a filtered data plot exhibiting reduced noise (fewer zigzag lines) compared to the unfiltered data plot. As depicted in the figure, the filtered line plot demonstrates a smoother profile while preserving the original height and width characteristics of the graph.

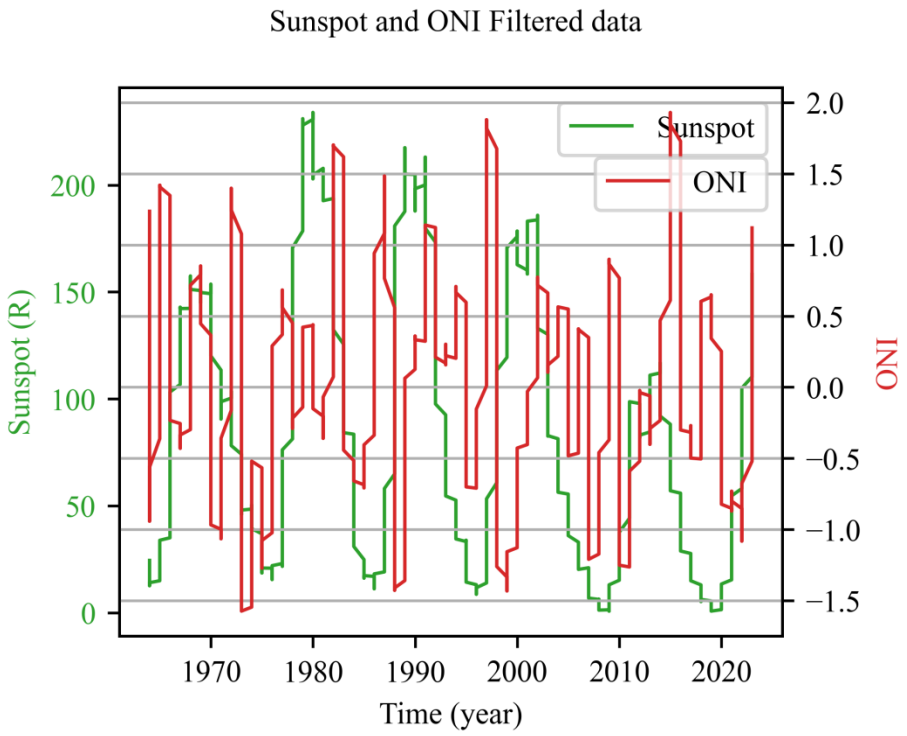

Figure 16: Time series Plot of Sunspot and ONI filtered data. Using a twin graph plot filtered data is present in time domain.

3.2.2. Fast Fourier Transform (FFT) of the data using a Periodogram

After removing the high-frequency components from the data, the resulting signal is transformed into the frequency domain using the Fast Fourier Transform (Cooley & Tukey, 1965). This transformation among others includes the periodogram technique in spectral analysis. The periodogram technique facilitates the examination of different signal frequencies to pinpoint prominent periodicities. It is particularly advantageous for identifying patterns or periodic fluctuations that may be obscured within complex or noisy time series datasets.

To implement the periodogram technique effectively, the time series data is typically segmented into overlapping segments and windowed to mitigate spectral leakage caused by abrupt transitions at segment boundaries or the use of square windows. Each segment of data is then

individually transformed into the frequency domain using the Fourier Transform. Subsequently, the transformed data from the different segments are averaged directly. The averaging process enhances the robustness of the estimation by reducing variance and the impact of noise.

The periodogram method, which was introduced by Bartlett (1950) and discussed by Unde and Shriram (2014), laid the foundation for the periodogram technique. This approach makes use of non-overlapping data segments to generate the frequency spectrum. In contrast, the Welch periodogram (Welch, 1967) emphasizes in the usage of overlapping segments. In general the Periodogram technique is essential for analyzing time series datasets, providing insights into their frequency characteristics and facilitating the identification of dominant periods. In this study, the Welch Periodogram technique is employed to compute and average energy spectra in the frequency domain to aid the identification of the prevalent frequency of El Niño and Sunspot.

Subsequently, the averaged spectra are evaluated for their energy content and visually compared by plotting them together on a single graph.

According to Hernandez, (1999), employing periodogram method is much more suitable for studying geophysical, astronomical and metrological observational datasets research (e.g., Dahlen & Simons, 2008; Donahue & Baliunas, 1992; Joshi et al., 2006; Lomb, 2013; Orr & Hoffman, 1974; Smirnov et al., 2005).

In using the periodogram technique, increasing the number of periodograms improves the suppression of false spectrums and enhances the accuracy of true ones. However, higher numbers of periodograms shorten the length of each dataset, affecting longer wavelength signals. Thus, it's crucial to balance data length against the number of periodograms. For this study, the optimal number of periodograms chosen was 20.

3.2.3. Coherency analysis

The coherence function can be calculated using the measured auto-spectral and cross-spectral density functions, which is a gauge of how accurate the presumed signals are correlated (Bendat & Piersol, 2011). Here we are going to calculate coherence using the measured auto-spectral and cross-spectral density functions as given in equation (2).

$$C_{xy}(\omega) = \frac{\sum_{i=0}^{n} X_i(\omega) \times Y_i^*(\omega)}{\sqrt{\sum_{i=0}^{n} |X_i(\omega)|^2 \times \sum_{i=0}^{n} |Y_i(\omega)|^2}}, \qquad (2)$$

Where ***** denotes complex conjugate, and $X_i(f)$ and $Y_i(f)$ are the fast Fourier transform (FFT) of the i^{th} segments in n overlapped windowed data segments of $X_i(k)$ and $Y_i(k)$, and $k = (1,2,3,\dots,N)$. Here $X_i(k)$ and $Y_i(k)$, are the solar cycle and ONI data sets respectively. Also, Equation (2) describe that the FFT of i^{th} term of the sunspot $X_i(f)$ signal multiplied by ONI signal$Y_i(f)$. For simplicity equation (2) can sometimes be written as that in equation (3)

$$C_{xy}(\omega) = \frac{S_{xy}(\omega)}{\sqrt{S_{xx}(\omega) * S_{yy}(\omega)}}, \qquad (3)$$

Where ω is the frequency and $S_{xx}(\omega)$ and $S_{yy}(\omega)$ are real quantities and $S_{xy}(\omega)$ is complex, it automatically follows that $C_{xy}(\omega)$ is a complex quantity with magnitude and argument. Here, the Welch Modified Periodogram approach has been applied (Rabiner & Gold, 1975; Welch, 1967). Typically, to replicate data at a specific frequency, divide each data set into k blocks and compute ${S_{xx}}^i(\omega)$, ${S_{yy}}^i(\omega)$ and ${S_{xy}}^i(\omega)$ where, $i = 1,2,\dots,k$.

Sometimes a magnitude-squared coherence between two signals is used to describe a real-valued function with the notion of coherence. Then the squared Coherency is calculated using equation (4).

$$\gamma^2(\omega) = |C_{xy}^2(\omega)|^2 = \frac{|S_{xy}(\omega)|^2}{S_{xx}(\omega) * S_{yy}(\omega)}. \quad (4)$$

Where, S_{xy} is the density of cross-spectral between x and y, and, S_{xx} and S_{yy} are the auto spectral density of x and y respectively.

The coherence functions must be carefully measured to evaluate the statistical confidence of frequency response function measurements. It is essential that the coherence results are consistently less than one (Bendat & Piersol, 2011). If any coherence function between two input records equals one, it indicates redundancy in the data. To address this issue, employing Welch's method, which involves segmenting data into blocks, is crucial (Bendat & Piersol, 2011). Additionally, Welch's power spectral estimation technique can be utilized to estimate the coherence function (Rabiner & Gold, 1975; Wang & Tang, 2004).

Using only one data segment or block will result in a coherence estimate of unity (1), regardless of the actual coherence value. Therefore, multiple segments are necessary. In this study, a total of 20 data segments, each containing 695 data points spanning from January 1964 to August 2023, were utilized. The data segmentation is carried out following the Welch method (Rabiner & Gold, 1975; Welch, 1967) and the coherence was calculated using equation (4). The squared coherence value, denoted as $\gamma^2(\omega)$, falls within the interval $0 \leq \gamma^2(\omega) \leq 1$. A value of $\gamma^2(\omega)$ closer to one indicates strong coherence between signals, whereas a value closer to zero suggests the signals are uncorrelated.

Since coherency values across all frequency ranges falls between 0 and 1, it was essential to establish a threshold to distinguish acceptable levels of correlation. To set this threshold value equation (5) has been utilized in this study.

$$C^2 = 1 - \alpha^{1/(n-1)}. \quad (5)$$

Where $\alpha = 1 - p$ and $p \times 100\%$ is the confidence threshold and n is the number of Periodograms or a number of data blocks (Julian, 1975; Thompson, 1979). This formula is very important to evaluate the coherence's significance. A coherence threshold is needed to identify the time intervals (period) or frequency bands where the signals are clearly cohereted. By generating a distribution of coherence from many surrogate data samples, this threshold of significant coherence can be identified. It is reasonable to utilize the 99^{th} percentile of the distribution as the threshold for a significance level of $\alpha = 0.01$ (Blaney et al., 2020).

3.2.4. Phase lag

Once the correlation between two signals is established, it becomes crucial to examine their phase lag. This reveals the extent of delay or phase shift between the signals across different frequencies, helping to determine which signal leads or lags at each frequency. This analysis is essential for understanding the temporal relationship between the signals across their frequency spectrum. Therefore, to determine, if there is a lag between the sunspot and El Niño we have to calculate their phase lag. The phase lag is calculated by using the imaginary and real part of $C_{xy}^2\ (f)$. The phase angle $\Theta_{xy}\ (f)$, between X (sunspot) and Y (ONI index) is estimated by:

$$\Theta_{xy}(f) = \tan^{-1}\left[\frac{Im\ (f)}{Re\ (f)}\right]. \qquad (6)$$

Phase lag, by itself, does not provide information about which event occurs before the other. However, in this study, consideration is made that the Sun is the ultimate or primary source of influence. It is widely recognized that the Earth's atmosphere is significantly impacted by the Sun's position and movement. This influence is fundamental because the Earth orbits the Sun and variations in solar radiation and other factors, will affect atmospheric dynamics. Therefore, when we discuss phase lag in relation to Sunspot counts and ONI data, we acknowledge that the Sun's influence on Earth's atmosphere is the cause of the lag. Given the acknowledged influence of the sun on the occurrence of El Niño events, it is essential to calculate the phase lag to comprehend the temporal relationship between these phenomena. A combined confidence interval for the gain and phase of the linear filter between X (sunspots in this work) and Y (ONI

in this work) is utilized to minimize residual variance and estimate the phase angle confidence interval (Jones & Nesmith). The phase lag index is determined by calculating the mean number of phase angle variations in the complex plane that point either upward or downward about the horizontal real axis (Cohen, 2015).

When the ratio of the coherence imaginary to real number is known, phase lag can be determined by finding the tangent inverse, also known as the tan inverse. The intercept and slop of the function are then determined by fitting the calculated ratio to a linear regression model. In order to calculate the linear regression, $y = a + bx$, model is needed, where x and y represent frequency and phase lag respectively. Then the estimated values of a and b are calculated as follows:

$$a = \frac{\sum y \sum x^2 - \sum x \sum xy}{n(\sum xy) - (\sum x)^2}, \quad (7)$$

$$b = \frac{n \sum xy - \sum x \sum y}{n \sum x^2 - (\sum x)^2}, \quad (8)$$

The estimated values for a and b will then be entered into the formula:

$$y = a + bx. \quad (9)$$

Finally, the slop (b) tells how much time lagged one event from the other. It is noteworthy that phase lags shorter than one month cannot be identified due to the resolution capacity of the data sets, which is one month. Interpretations of the data should therefore take this constraint into account.

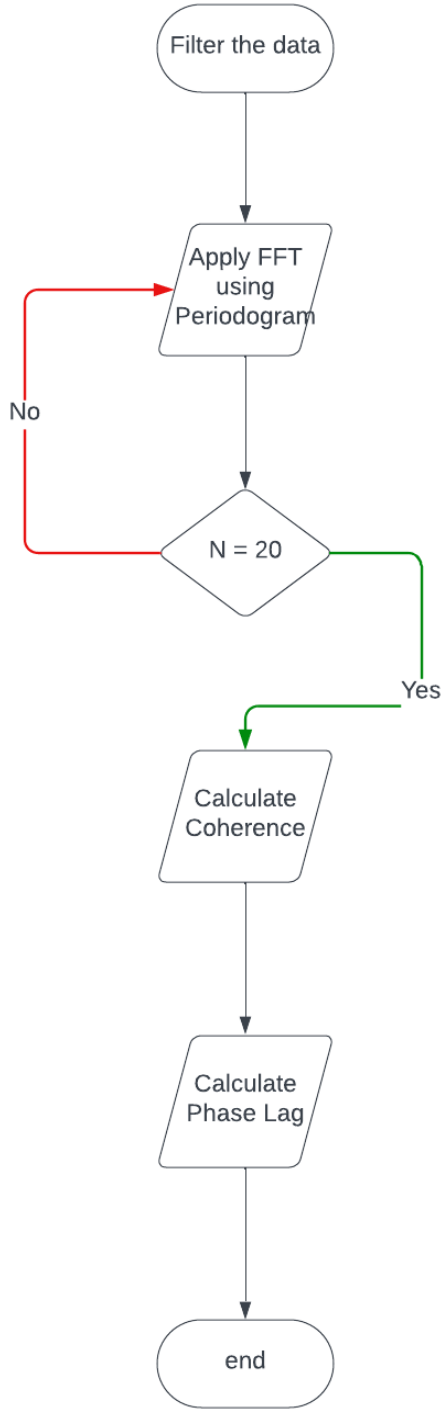

Figure 17: Flow chart of data processing

The steps taken in the data processing are shown in the flow chart above. Furthermore, it provided clear steps of all data processing methods.

Data processing procedures and methods are depicted in the flow chart above. It also demonstrated data processing in its entirety and its methodology in a clear manner. To investigate the connection between solar activity and ENSO, all of the abovementioned statistical techniques were taken into account. I used the Python programming language for this study paper. Reliable software such as Matlab, Python, and others can perform all of the aforementioned statistical techniques and their wave nature of signal processing. Still, the software operates based on scientific theory and statistical approach notions.

CHAPTER 4

4. RESULT AND DISCUSSION

4.1.Result

Figure 18 illustrates the amplitude spectrum plot, depicting data for both Sunspot and ONI. Upon inspection of Figure 18, it is evident that the dominant magnitude values of frequencies reside predominantly within the frequency range below 0.3 Hz. This implies that the frequencies of greatest significance are concentrated below the frequency of 0.3 Hz. Consequently, to enable a more comprehensive analysis of the frequency correlation between sunspot and ONI data, Figure (19) is presented as an enlarged or zoomed-in version of Figure (18). This plot focuses specifically on the frequency range from 0 to 0.3 Hz. This representation aimed at providing a clearer analysis of the frequency relationship between these two datasets.

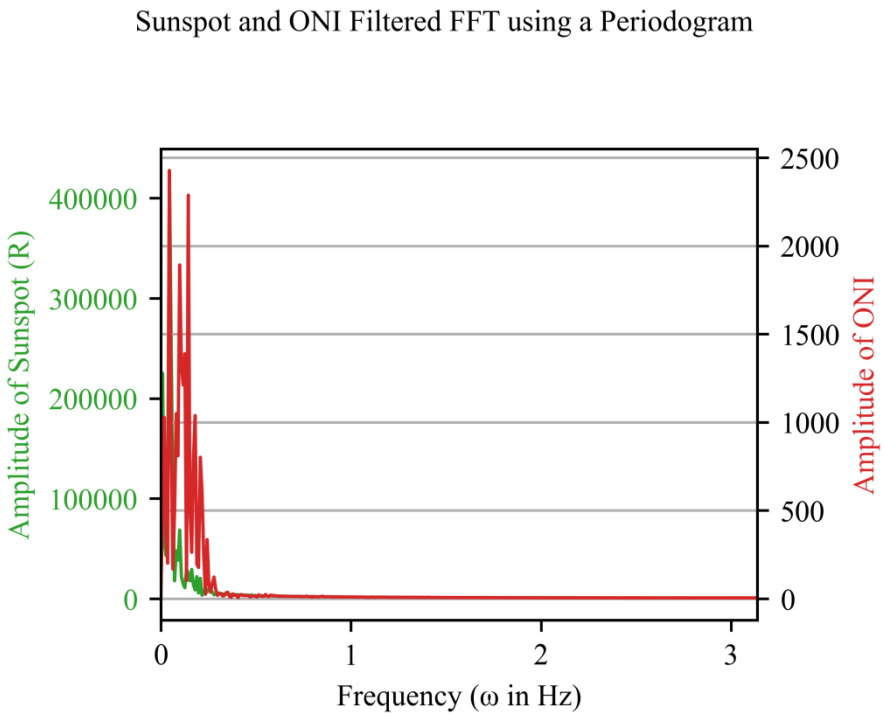

Figure 18: The amplitude spectrum of the Sunspot and ONI data using the FFT method.

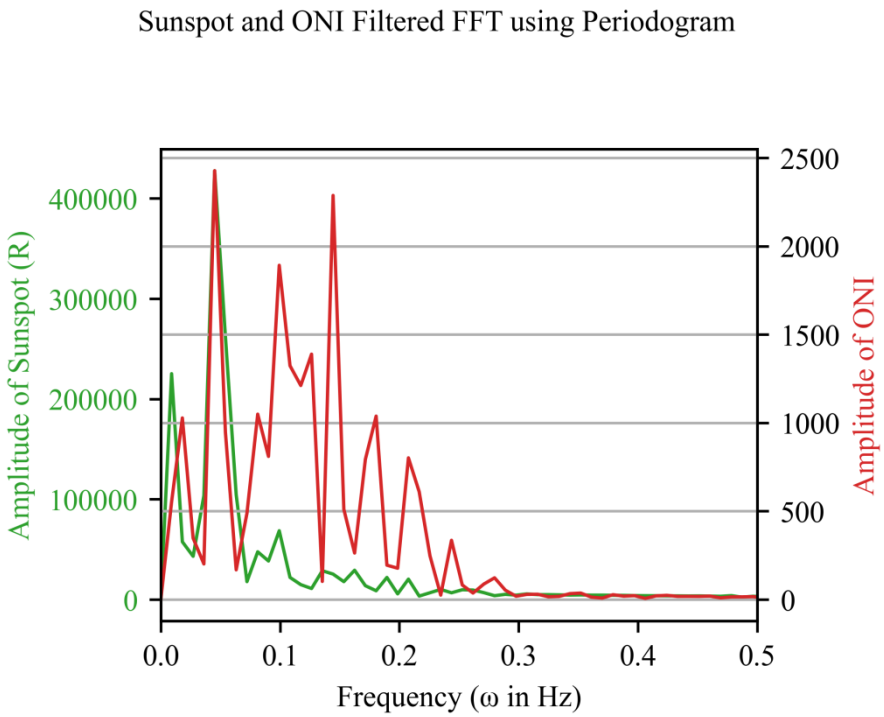

Figure 19: The amplitude spectrum of the Sunspot and ONI data using the FFT method, in the range between 0 and 0.3Hz.

As it can be seen in Figure (19) the strongest correlation is observed at the frequency ω = 0.04513783, where both datasets exhibit maximum amplitudes in the frequency domain. This frequency represents the most prominent alignment between sunspot and ONI data. Additionally, there are other notable frequencies where correlations between the datasets are observed, specifically at ω = 0.08124809, ω = 0.09930322, and ω = 0.207634. In general Figure (19) provides a detailed depiction of these frequency correlations, highlighting both commonalities and distinctive features between sunspot and ONI datasets across various frequencies.

Furthermore, there are frequencies with significant amplitudes that are distinctive to either El Niño or sunspot events. For instance, the frequency ω = 0.00902757 highlights the amplitude associated solely with sunspots. In contrast, the frequencies ω = 0.01805513, ω = 0.12638591, ω = 0.14444104, ω = 0.1805513, and ω = 0.24374426 indicate amplitudes in the ONI dataset, showcasing variations specific to the El Niño phenomenon.

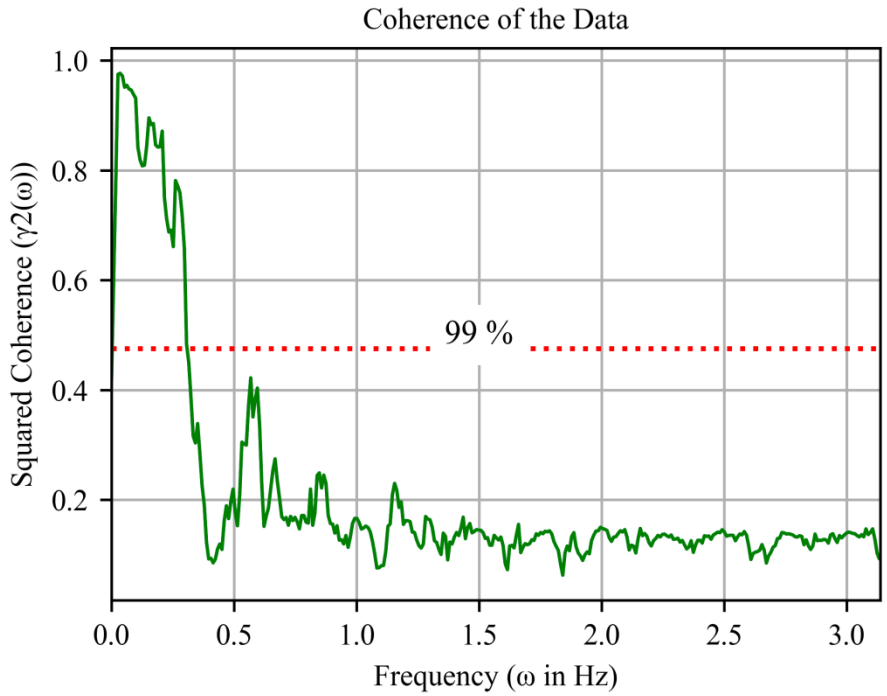

Figure 20: The coherence between the sunspot count and ONI data.

Furthermore, to assess the strength of correlation between amplitudes across different frequencies, the coherency between the two signals was computed using the methodology outlined in the methodology section and depicted in Figure (20). As shown in Figure (20), the results of the coherency analysis align closely with those of Figure (19), illustrating a robust correlation in the frequency domain between sunspot counts and ONI data. Figure (20) indicates that the coherency values between the signals are predominantly close to 1, suggesting a strong correlation particularly in the lower frequency or longer wavelength ranges.

To determine which coherency values are statistically significant, Equation (5) was employed (Julian, 1975; Thompson, 1979) with a confidence level of 99% and 695 measurement points (n), establishing a threshold value 0.464. The most significant coherency is observed at the frequency $\omega = 0.04513783$, with a squared coherency value of 0.97. Additionally, notable coherency values are observed at frequencies $\omega = 0.09930322$, $\omega = 0.1534686$, $\omega = 0.17152373$, $\omega = 0.2076339$, $\omega = 0.23471669$, and $\omega = 0.26179930$, all exceeding the 99% threshold, indicating significant correlation between the two signals at these frequencies.

Figure (20) also shows additional points that exhibit correlation, but they do not meet the confidence criterion and thus cannot be considered coherent.

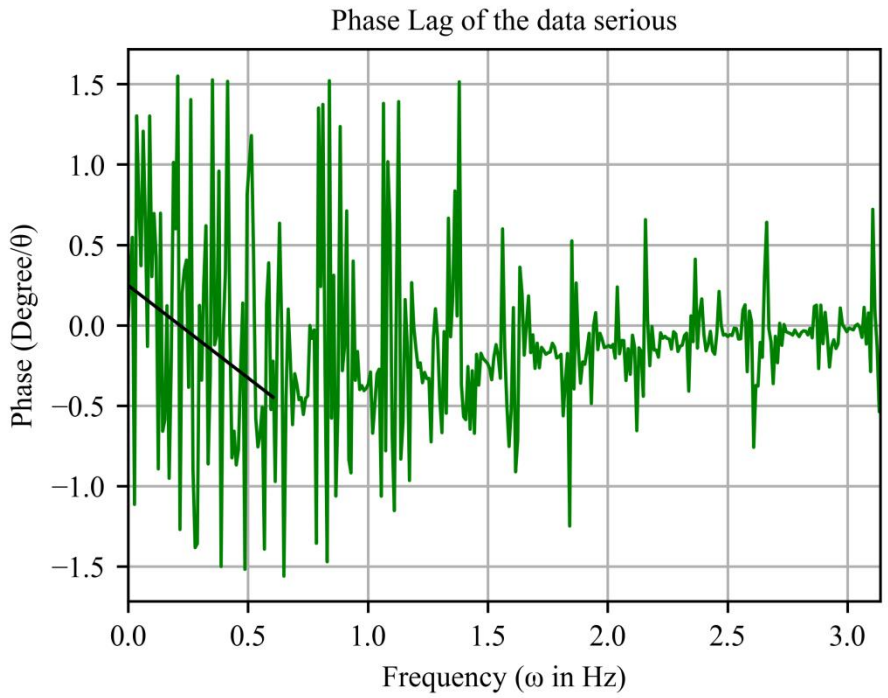

Figure 21: Phase Lag between the Sunspot count and ONI data

After determining the coherency between the two signals, the next step involved analyzing whether there is a time delay between sunspot activity and the onset of El Niño. To accomplish this, the phase angle was computed as described in Equation (6), taking into consideration the resolution of the data. Figure (21) presents the phase angle between sunspot counts and El Niño data.

Subsequently, a linear regression analysis was performed to fit a straight line to the phase angle data, as detailed in the methodology section. The resulting line has a slope of -1.08895449 and a y-intercept of 0.34427296, indicating that it accurately represents the relationship. This equation takes the form: $\theta(t) = -1.08895449\ (t) + 0.34427296$. Here the slope of the curve represents phase lag between the two data sets.

4.2.Discussion

The close analysis of the Sunspot count and ONI data in the frequency domain has already revealed that there is a correlation between them, in different frequency bands. To calculate the periods at which the two signals are correlated one can calculate the period from the frequencies using equation (10).

$$T = \frac{2\pi}{\omega}. \qquad (10)$$

Equation (10) is employed to calculate the recurrence periods of solar cycle and ENSO events based on the frequencies obtained from the visual comparison and coherency analysis. For instance, the frequency ω = 0.00902757 corresponds to a period of 57.99 years, which is the period associated with the influx of interplanetary dust particles into Earth's atmosphere that can influence climate conditions (Scafetta et al., 2020; Veretenenko & Ogurtsov, 2018)

Peak of Figure (19) unequivocally demonstrates that the frequency at which both signals are attaining a maximum amplitude is at ω = 0.04513783, or a period of 11.59 years. In comparison to amplitudes at other frequencies or periods, El Niño and Sunspot counts show their highest amplitudes at this 11.59-year period. It is also widely acknowledged that this period is an important solar cycle phase (Hathaway, 2015; Stager et al., 2007).

Each solar cycle lasts around 11.6 years. This time indicates the end of the previous cycle and the beginning of the new solar cycle. The end of the solar cycle can impact the influx of cosmic rays into the Earth's atmosphere. During solar minimum, cosmic ray intensity that enters the Earth's atmosphere is at its peak. This is because there is less protection from galactic cosmic rays during solar minimum due to the lower interplanetary magnetic field and solar wind (Usoskin et al., 2004). As the solar cycle ends and solar activity decreases, cosmic ray levels can potentially rise. Cosmic rays can have interactions with atmospheric particles and cloud formation, potentially affecting cloud properties and atmospheric processes (Svensmark & Friis-Christensen, 1997).

Similarly, ω = 0.08124809, ω = 0.09930322, and ω = 0.207634 correspond to time periods of T = 6.44 years, T = 5.27 years, and T = 2.52 years respectively. These periods are common for both ONI index (orange line plot) and the solar cycle (green line plot) on Figure (19).

The periods, namely T = 5.27 shows half solar cycle (the peak period of solar cycle) where the activity of the Sun will be maximum (Hathaway, 2015). During this time, on the Sun, several phenomena such as CMEs and various types of flares manifest themselves at solar maximum. Furthermore, the Earth's atmosphere may be impacted by these high energy events. The sun's activity during solar maximum may therefore be the cause of these periods. In order to conclude several physical parameters of both events should be studied well.

The remaining peaks in Figure (19) are observed either in the ENSO events (orange line plot) or in sunspot activity (green line plot), but not both. Frequencies such as ω = 0.01805513, ω = 0.12638591, ω = 0.14444104, ω = 0.1805513, and ω = 0.24374426 are exclusively associated with ENSO events. These frequencies correspond to periods of T = 29 years, and the rest periods lays between in the range of 7-2 years (e.g., Enfield, 1989; McPhaden, 2002; Philander, 1985; Philander, 1998; Ray & Giese, 2012; Trenberth, 1997; Wolde-Georgis, 1997) these are T = 4.1428 years, T = 3.625 years, T = 2.9 years, and T = 2.148 years, which are roughly El Niño periods documented in the literature. The 29-year period is related to the Inter-decadal Pacific oscillation (IPO) cycle, which is around 15-30 years (Folland et al., 2002). It is an important factor in understanding and predicting long-term changes in global and regional climate patterns beyond the typical ENSO timescales (Salinger et al., 2001). The warm (positive) IPO phase is associated with more frequent and stronger El Niño events, while the cool (negative) IPO phase is linked to more frequent and stronger La Niña events (Folland et al., 2002). The IPO phase influences global and regional climate patterns, including temperature, precipitation, and storm activity in many parts of the world (Dong & Dai, 2015).

As depicted in Figure (20), there is a strong coherency between the Sunspot and ONI index data, with coherence values ranging from 0.97 to 0.68 across frequencies from 0.009 Hz to 0.3 Hz. Within these frequency ranges, distinct peaks indicate clear correlations between the two signals.

Specifically, peak coherencies are observed at frequencies such as ω = 0.0451378, ω = 0.0993032, ω = 0.1534686, ω = 0.1715237, ω = 0.2076339, ω = 0.2347166, and ω = 0.2617993, corresponding to periods of T = 11.6 years, T = 5.2 years, T = 3.41 years, T = 3.05 years, T = 2.55 years, T = 2.23 years, and T = 2 years respectively. These periods are roughly associated with both El Niño and solar cycle periods (see e.g., Hathaway, 2015; Hathaway & Wilson, 2004; Philander, 1998).

For the period T = 11.6 year, T = 5.2 year, T = 3.41 year, T = 3.05 year, T = 2.55 year, T = 2.23 year and T = 2 year the value of coherency is $\gamma^2(\omega) = 0.97$, $\gamma^2(\omega) = 0.93$, $\gamma^2(\omega) = 0.89$, $\gamma^2(\omega) = 0.88$, $\gamma^2(\omega) = 0.87$, $\gamma^2(\omega) = 0.68$, and $\gamma^2(\omega) = 0.78$ respectively.

The results of the coherency analysis indicate that the period T = 11.6 years shows the highest coherence between the Solar cycle and ENSO events. This period signifies the transition between the end of one solar cycle and the beginning of the next. During this phase, the Sun's activity decreases, sometimes resulting in periods of low or no solar activity. As a result, the strength of the Earth magnetic field weakens, allowing cosmic rays and other particles to penetrate the atmosphere intensively. This influx of cosmic rays can potentially impact cloud formation, as well as various atmospheric processes on Earth (Rycroft et al., 2000 ; Svensmark, 2007).

As indicated previously the T = 5.2 year period is linked as the half period of the solar maximum. The duration of the time indicates that it is half of the solar cycle, and that the solar cycle is in its active phase, or the solar maximum, during this phase. Additionally, the sun is active at this time, causing a variety of phenomena to emerge that are quite likely to have an impact on Earth's atmosphere.

Figure (21) shows the phase angle relationship between solar cycle and ENSO events. The phase lag can be computed across frequencies from 0 Hz to 0.6 Hz, which showed an apparent decrease that can be fitted by a linear curve. Using linear regression, the slope and intercept of this trend were calculated, yielding a slope of m = -1.08895449. This indicates a delay of approximately

one month between solar activity and the onset of ENSO events. However, it is important to note that the data resolution is one month, meaning any lag shorter than one month cannot be accurately resolved. Therefore, this finding should not be considered conclusive.

Moreover, the delay only indicates the time difference between the occurrences of the two events but does not specify which event occurred first or which one follows. Therefore, establishing a cause-effect relationship solely from this analysis only is challenging. Nevertheless, considering the Sun as the primary and ultimate energy source for the Earth, it is reasonable to infer that the El Niño phase begins after the occurrence of the solar cycle event. Taking the data resolution into full consideration one can conclude that ENSO event tends to occur few days to one month after the end of each solar cycle. The delay however, can be properly determined using high resolution data sets.

CHAPTER 5

5. CONCLUSION AND RECOMMENDATION

5.1. Conclusion

This study aimed at investigating the relationship between the solar cycle and ENSO using data from Sunspot counts and ONI, respectively. Initially, the data underwent though filtering and frequency domain transformation using the Welch periodogram in the FFT. Later, visual comparisons of the amplitude spectrum of both signals were conducted, followed by coherency analysis to assess their correlation. The findings from this research have resulted in the following conclusions that the visual inspection of both datasets reveals peaks at multiple periods, from which the prominent amplitude occur at the approximate period of 11.59 years. The coherence analysis also demonstrated a strong correlation between solar cycles and ENSO events across various periods, notably at 11.59 years, corresponding to one solar cycle. This correlation is significant, showing a coherence level of 99% in several instances. Furthermore, there are significant correlations between the two datasets across various frequency spectrums, particularly notable coherence exists near the half of the solar cycle period, second only to the 11.59-year cycle.

Given the sun's role as Earth's primary energy source and prior research indicating solar phenomena commonly impact climate, coupled with observed phase lags, ENSO events are inferred to typically occur several days to one month after the conclusion of each solar cycle. Furthermore, the study underscores the inseparable connection between solar activity and ENSO events, emphasizing the pivotal role of the sun in influencing Earth's atmosphere.

In general, these studies highlight the compelling relationship between solar cycles and ENSO, opening the door for further investigation into additional physical parameters that may enhance our understanding of this complex interaction

5.2. Recommendation

A thorough examination of several physical characteristics related to the solar cycle and El Niño is necessary to get further insights and understanding of these phenomena. Additionally, it's a good idea to compute the phase lag using daily data if the ONI data is available since this will make it easier to see the phase lag within a set number of days. The results of the research will primarily serve as input for the climate forecasting unit once the aforementioned criteria have been thoroughly examined. Given the accuracy of El Niño forecasts, it will be imperative for many entities, including the Ministry of Agriculture and the Metrology Institute, to modify their strategies and policies in accordance with the latest scientific findings.

Reference

Bartlett, M. S. (1950). Periodogram analysis and continuous spectra. *Biometrika*, *37*(1/2), 1-16.

Bendat, J. S., & Piersol, A. G. (2011). *Random data: analysis and measurement procedures*. John Wiley & Sons.

Bieber, J. W., Chen, J., Matthaeus, W. H., Smith, C. W., & Pomerantz, M. A. (1993). Long-term variations of interplanetary magnetic field spectra with implications for cosmic ray modulation. *Journal of Geophysical Research: Space Physics*, *98*(A3), 3585-3603.

Blaney, G., Sassaroli, A., & Fantini, S. (2020). Algorithm for determination of thresholds of significant coherence in time-frequency analysis. *Biomedical signal processing and control*, *56*, 101704.

Bocchialini, K., Grison, B., Menvielle, M., Chambodut, A., Cornilleau-Wehrlin, N., Fontaine, D., Marchaudon, A., Pick, M., Pitout, F., & Schmieder, B. (2018). Statistical analysis of solar events associated with storm sudden commencements over one year of solar maximum during cycle 23: Propagation from the Sun to the Earth and effects. *Solar Physics*, *293*(5), 75.

Bravo, S., Stewart, G., & Blanco-Cano, X. (1998). The varying multipolar structure of the Sun's magnetic field and the evolution of the solar magnetosphere through the solar cycle. *Solar Physics*, *179*, 223-235.

Brovkin, V., Sitch, S., Von Bloh, W., Claussen, M., Bauer, E., & Cramer, W. (2004). Role of land cover changes for atmospheric CO2 increase and climate change during the last 150 years. *Global Change Biology*, *10*(8), 1253-1266.

Cane, H., Wibberenz, G., Richardson, I., & Von Rosenvinge, T. (1999). Cosmic ray modulation and the solar magnetic field. *Geophysical Research Letters*, *26*(5), 565-568.

Cohen, M. X. (2015). Effects of time lag and frequency matching on phase-based connectivity. *Journal of neuroscience methods*, *250*, 137-146.

Cooley, J. W., & Tukey, J. W. (1965). An algorithm for the machine calculation of complex Fourier series. *Mathematics of computation*, *19*(90), 297-301.

Courtillot, V., Gallet, Y., Le Mouël, J.-L., Fluteau, F., & Genevey, A. (2007). Are there connections between the Earth's magnetic field and climate? *Earth and Planetary Science Letters*, *253*(3-4), 328-339.

Crowley, T. J. (2000). Causes of climate change over the past 1000 years. *Science*, *289*(5477), 270-277.

Dahlen, F., & Simons, F. J. (2008). Spectral estimation on a sphere in geophysics and cosmology. *Geophysical Journal International*, *174*(3), 774-807.

Diro, G. T., Grimes, D., & Black, E. (2011). Large scale features affecting Ethiopian rainfall. *African Climate and Climate Change: Physical, Social and Political Perspectives*, 13-50.

Donahue, R. A., & Baliunas, S. L. (1992). Periodogram analysis of 240 years of sunspot records. *Solar Physics*, *141*, 181-197.

Dong, B., & Dai, A. (2015). The influence of the interdecadal Pacific oscillation on temperature and precipitation over the globe. *Climate dynamics*, *45*, 2667-2681.

Eltahir, E. A. (1996). El Niño and the natural variability in the flow of the Nile River. *Water Resources Research*, *32*(1), 131-137.

Enfield, D. B. (1989). El Niño, past and present. *Reviews of geophysics*, *27*(1), 159-187.

Folland, C., Renwick, J., Salinger, M., & Mullan, A. (2002). Relative influences of the interdecadal Pacific oscillation and ENSO on the South Pacific convergence zone. *Geophysical Research Letters*, *29*(13), 21-21-21-24.

Friedli, T. K. (2020). Recalculation of the Wolf Series from 1877 to 1893. *Solar Physics*, *295*(6), 72.

Gallagher, N. B. (2020). Savitzky-Golay smoothing and differentiation filter. *Eigenvector Research Incorporated*.

Gibbard, S., Caldeira, K., Bala, G., Phillips, T. J., & Wickett, M. (2005). Climate effects of global land cover change. *Geophysical Research Letters*, *32*(23).

Glantz, M. H. (2001). Currents of change: impacts of El Niño and La Niña on climate and society. Cambridge University Press.

Glantz, M. H., & Ramirez, I. J. (2020). Reviewing the Oceanic Niño Index (ONI) to enhance societal readiness for El Niño's impacts. *International Journal of Disaster Risk Science*, *11*, 394-403.

Grove, R., & Adamson, G. (2018). *El Niño in world history*. Springer.

Guiñón, J. L., Ortega, E., García-Antón, J., & Pérez-Herranz, V. (2007). Moving average and Savitzki-Golay smoothing filters using Mathcad. *Papers ICEE*, *2007*, 1-4.

Hammer, G. L., Nicholls, N., & Mitchell, C. (2000). *Applications of seasonal climate forecasting in agricultural and natural ecosystems* (Vol. 21). Springer Science & Business Media.

Hamming, R. W. (1998). *Digital filters*. Courier Corporation.

Hanley, D. E., Bourassa, M. A., O'Brien, J. J., Smith, S. R., & Spade, E. R. (2003). A quantitative evaluation of ENSO indices. *Journal of Climate*, *16*(8), 1249-1258.

Harvey, K. L., & White, O. R. (1999). What is solar cycle minimum? *Journal of Geophysical Research: Space Physics*, *104*(A9), 19759-19764.

Hathaway, D. H. (2015). The solar cycle. *Living reviews in solar physics*, *12*, 1-87.

Hathaway, D. H., & Wilson, R. M. (2004). What the sunspot record tells us about space climate. *Solar Physics*, *224*(1-2), 5-19.

Hedgecock, P. (1975). Measurements of the interplanetary magnetic field in relation to the modulation of cosmic rays. *Solar Physics*, *42*, 497-527.

Hernandez, G. (1999). Time series, periodograms, and significance. *Journal of Geophysical Research: Space Physics*, *104*(A5), 10355-10368.

Jones, B. E., & Nesmith, T. D. COHERENCE ANALYSIS.

Joshi, B., Pant, P., & Manoharan, P. (2006). Periodicities in sunspot activity during solar cycle 23. *Astronomy & Astrophysics*, *452*(2), 647-650.

Juckett, D. A. (2010). Evidence for possible interactions between the solar wind and global sea surface temperatures (SST). *Journal of Atmospheric and Solar-Terrestrial Physics*, *72*(9-10), 801-805.

Julian, P. R. (1975). Comments on the determination of significance levels of the coherence statistic. *Journal of the Atmospheric Sciences*, *32*(4), 836-837.

Kessler, W. S. (2002). Is ENSO a cycle or a series of events? *Geophysical Research Letters*, *29*(23), 40-41-40-44.

Kim, H.-M., Webster, P. J., & Curry, J. A. (2011). Modulation of North Pacific tropical cyclone activity by three phases of ENSO. *Journal of Climate*, *24*(6), 1839-1849.

Kirov, B., & Georgieva, K. (2002). Long-term variations and interrelations of ENSO, NAO and solar activity. *Physics and Chemistry of the Earth, Parts a/B/C*, *27*(6-8), 441-448.

Klotzbach, P. J. (2011). El Niño–Southern Oscillation's impact on Atlantic basin hurricanes and US landfalls. *Journal of Climate*, *24*(4), 1252-1263.

Kunjaya, C., Radiman, I., Dupe, Z., Herdiwijaya, D., & Hakim, M. (2001). Are El Niño and La Niña Phenomena Influenced by Solar Activities. *JMS*, *6*(1).

Lanza, R., & Meloni, A. (2006). *The Earth's Magnetic Field*. Springer.

L'Heureux, M. L., Levine, A. F., Newman, M., Ganter, C., Luo, J. J., Tippett, M. K., & Stockdale, T. N. (2020). ENSO prediction. *El Niño Southern Oscillation in a changing climate*, 227-246.

Lee, C., Luhmann, J., Hoeksema, J., Sun, X., Arge, C., & de Pater, I. (2011). Coronal field opens at lower height during the solar cycles 22 and 23 minimum periods: IMF comparison suggests the source surface should be lowered. *Solar Physics*, *269*, 367-388.

Lefèvre, L., & Clette, F. (2011). A global small sunspot deficit at the base of the index anomalies of solar cycle 23. *Astronomy & Astrophysics*, *536*, L11.

Lomb, N. (2013). The sunspot cycle revisited. Journal of Physics: Conference Series,

Lourens, L. J. (2021). The variation of the Earth's movements (orbital, tilt, and precession) and climate change. In *Climate change* (pp. 583-606). Elsevier.

McPhaden, M. J. (2002). El Niño and La Niña: causes and global consequences. *Encyclopedia of global environmental change*, *1*, 353-370.

Mikhaylov, A., Moiseev, N., Aleshin, K., & Burkhardt, T. (2020). Global climate change and greenhouse effect. *Entrepreneurship and Sustainability Issues*, *7*(4), 2897.

Mordvinov, A. V., Pevtsov, A. A., Bertello, L., & Petrie, G. J. (2016). The reversal of the Sun's magnetic field in cycle 24. *arXiv preprint arXiv:1602.02460*.

Mumtahana, F., Sulistiani, S., & Kesumaningrum, R. (2015). Correlation between solar activity and El Niño Southern Oscillation (ENSO). AIP Conference Proceedings,

Nguyen, V., & Dorka, U. (2008). Phase lag compensation in real-time substructure testing based on online system identification. Proc. 14th World Conf. on Earthquake Engineering,

Orr, W. C., & Hoffman, H. J. (1974). A 90-Min Cardiac Biorhythm Methodology and Data Analysis Using Modified Periodograms and Complex Demodulation. *IEEE Transactions on Biomedical Engineering*(2), 130-143.

Philander, S. (1985). El Niño and La Niña. *Journal of Atmospheric Sciences*, *42*(23), 2652-2662.

Philander, S. G. (1998). Who is El Niño? *Eos, Transactions American Geophysical Union*, *79*(13), 170-170.

Pielke Jr, R. A., & Landsea, C. N. (1999). La nina, el nino, and atlantic hurricane damages in the united states. *Bulletin of the American Meteorological Society*, *80*(10), 2027-2034.

Pielke Sr, R. A., Pitman, A., Niyogi, D., Mahmood, R., McAlpine, C., Hossain, F., Goldewijk, K. K., Nair, U., Betts, R., & Fall, S. (2011). Land use/land cover changes and climate: modeling analysis and observational evidence. *Wiley Interdisciplinary Reviews: Climate Change*, *2*(6), 828-850.

Press, W. H., & Teukolsky, S. A. (1990). Savitzky-Golay smoothing filters. *Computers in Physics*, *4*(6), 669-672.

Rabiner, L. R., & Gold, B. (1975). Theory and application of digital signal processing. *Englewood Cliffs: Prentice-Hall*.

Rader, C. M., & Gold, B. (1967). Digital filter design techniques in the frequency domain. *Proceedings of the IEEE*, *55*(2), 149-171.

Radiman, I., Herdiwidjaja, D., Dupe, Z. L., Kunjaya, C., & Hakim, M. I. (2009). Solar Cycle Variations and its Effects on El Niño/La Niña Behaviour. *Jurnal Matematika & Sains*, *8*(2), 47-50.

Ray, S., & Giese, B. S. (2012). Historical changes in El Niño and La Niña characteristics in an ocean reanalysis. *Journal of Geophysical Research: Oceans*, *117*(C11).

Richardson, I., Cliver, E., & Cane, H. (2001). Sources of geomagnetic storms for solar minimum and maximum conditions during 1972–2000. *Geophysical Research Letters*, *28*(13), 2569-2572.

Rodrigues, R. R., & McPhaden, M. J. (2014). Why did the 2011–2012 La Niña cause a severe drought in the Brazilian Northeast? *Geophysical Research Letters*, *41*(3), 1012-1018.

Salinger, M., Renwick, J. A., & Mullan, A. (2001). Interdecadal Pacific oscillation and south Pacific climate. *International journal of climatology: a journal of the Royal Meteorological Society*, *21*(14), 1705-1721.

Savitzky, A., & Golay, M. J. (1964). Smoothing and differentiation of data by simplified least squares procedures. *Analytical chemistry*, *36*(8), 1627-1639.

Scafetta, N., Milani, F., & Bianchini, A. (2020). A 60-year cycle in the Meteorite fall frequency suggests a possible interplanetary dust forcing of the Earth's climate driven by planetary oscillations. *Geophysical Research Letters*, *47*(18), e2020GL089954.

Schafer, R. W. (2011). What is a Savitzky-Golay filter?[lecture notes]. *IEEE Signal processing magazine*, *28*(4), 111-117.

Schuster, A. (1898). On the investigation of hidden periodicities with application to a supposed 26 day period of meteorological phenomena. *Terrestrial Magnetism*, *3*(1), 13-41.

Seleshi, Y., Demaree, G., & Delleur, J. (1994). Sunspot numbers as a possible indicator of annual rainfall at Addis Ababa, Ethiopia. *International Journal of climatology*, *14*(8), 911-923.

Smirnov, V., Ponomarev, A., Jiadong, Q., & Cherepantsev, A. (2005). Rhythms and deterministic chaos in geophysical time series. *IZVESTIIA PHYSICS OF THE SOLID EARTH C/C OF FIZIKA ZEMLI-ROSSIISKAIA AKADEMIIA NAUK*, *41*(6), 428.

Stager, J. C., Ruzmaikin, A., Conway, D., Verburg, P., & Mason, P. J. (2007). Sunspots, el nino, and the levels of lake victoria, east africa. *Journal of Geophysical Research: Atmospheres*, *112*(D15).

Stix, M. (1981). Theory of the solar cycle. *Solar Physics*, *74*, 79-101.

Su, J., Zhang, R., Li, T., Rong, X., Kug, J., & Hong, C.-C. (2010). Causes of the El Niño and La Niña amplitude asymmetry in the equatorial eastern Pacific. *Journal of Climate*, *23*(3), 605-617.

Svalgaard, L., Cagnotti, M., & Cortesi, S. (2017). The effect of sunspot weighting. *Solar Physics*, *292*(2), 34.

Rycroft, M., Israelsson, S., & Price, C. (2000). The global atmospheric electric circuit, solar activity and climate change. *Journal of Atmospheric and Solar-Terrestrial Physics*, *62*(17-18), 1563-1576.

Svensmark, H., & Friis-Christensen, E. (1997). Variation of cosmic ray flux and global cloud coverage—a missing link in solar-climate relationships. *Journal of Atmospheric and Solar-Terrestrial Physics*, *59*(11), 1225-1232.

Thompson, R. O. (1979). Coherence significance levels. *Journal of the Atmospheric Sciences*, *36*(10), 2020-2021.

Trenberth, K. E. (1997). The definition of el nino. *Bulletin of the American Meteorological Society*, *78*(12), 2771-2778.

Trenberth, K. E., & Hoar, T. J. (1997). El Niño and climate change. *Geophysical Research Letters*, *24*(23), 3057-3060.

Unde, S. A., & Shriram, R. (2014). Coherence analysis of EEG signal using power spectral density. 2014 Fourth International Conference on Communication Systems and Network Technologies,

Usoskin, I., & Mursula, K. (2003). Long-term solar cycle evolution: review of recent developments. *Solar Physics*, *218*, 319-343.

Usoskin, I., Gladysheva, O., & Kovaltsov, G. (2004). Cosmic ray-induced ionization in the atmosphere: spatial and temporal changes. *Journal of Atmospheric and Solar-Terrestrial Physics*, *66*(18), 1791-1796.

Usoskin, I. G. (2017). A history of solar activity over millennia. *Living reviews in solar physics*, *14*(1), 3.

Uzal, L. C., Piacentini, R., & Verdes, P. F. (2012). Predictions of the maximum amplitude, time of occurrence, and total length of solar cycle 24. *Solar Physics*, *279*, 551-560.

Vérard, C., Hochard, C., Baumgartner, P. O., Stampfli, G. M., & Liu, M. (2015). Geodynamic evolution of the Earth over the Phanerozoic: Plate tectonic activity and palaeoclimatic indicators. *Journal of Palaeogeography*, *4*(2), 167-188.

Veretenenko, S., & Ogurtsov, M. (2018). 60-year cycle in the Earth's climate and dynamics of correlation links between solar activity and circulation of the lower atmosphere. *Geomagnetism and Aeronomy*, *58*, 973-981.

Wang, S., & Tang, M. (2004). Exact confidence interval for magnitude-squared coherence estimates. *IEEE signal processing letters*, *11*(3), 326-329.

Weiher, R. F. (2000). Improving El Niño forecasting: the potential economic benefits.

Welch, P. (1967). The use of fast Fourier transform for the estimation of power spectra: A method based on time averaging over short, modified periodograms. *IEEE Transactions on audio and electroacoustics*, *15*(2), 70-73.

Williams, C. J., & Kniveton, D. R. (2011). *African climate and climate change: physical, social and political perspectives* (Vol. 43). Springer Science & Business Media.

Wolde-Georgis, T. (1997). El Nino and drought early warning in Ethiopia. *Internet Journal of African Studies*(2).

Zhai, Q. (2017). Evidence for the effect of sunspot activity on the El Niño/Southern Oscillation. *New Astronomy*, *52*, 1-7.

Zhou, Q., Chen, W., & Zhou, W. (2013). Solar cycle modulation of the ENSO impact on the winter climate of East Asia. *Journal of Geophysical Research: Atmospheres*, *118*(11), 5111-5119.

Appendices

A-Time series data

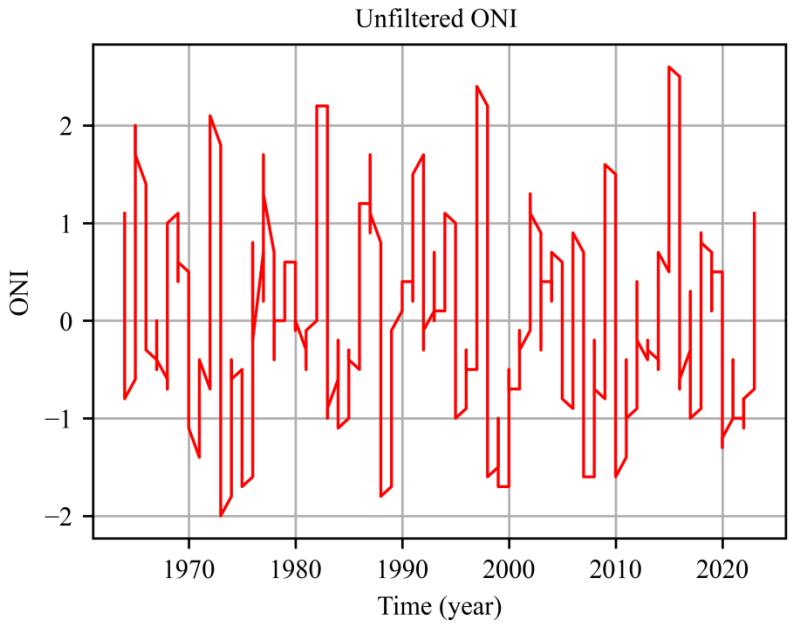

Figure 22: ONI of the data in yearly time Series

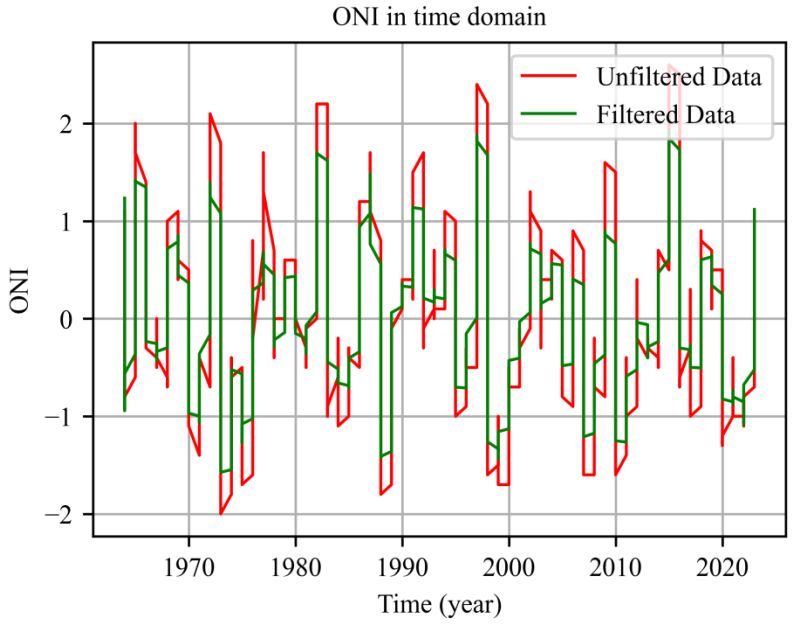

Figure 23: Filtered data of ONI, illustrates how the data's noise has been removed.

B-Frequency domain data

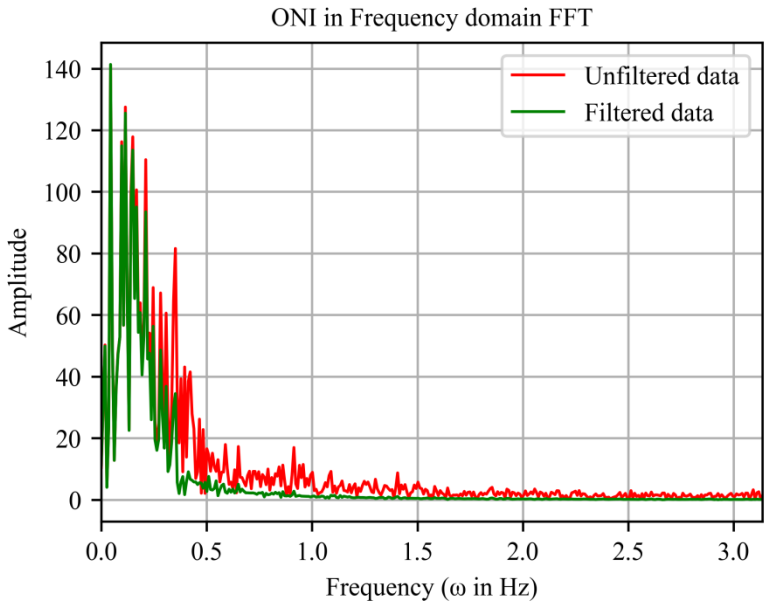

Figure 24: The amplitude spectrum of ONI Unfiltered and Filtered data using the FFT method

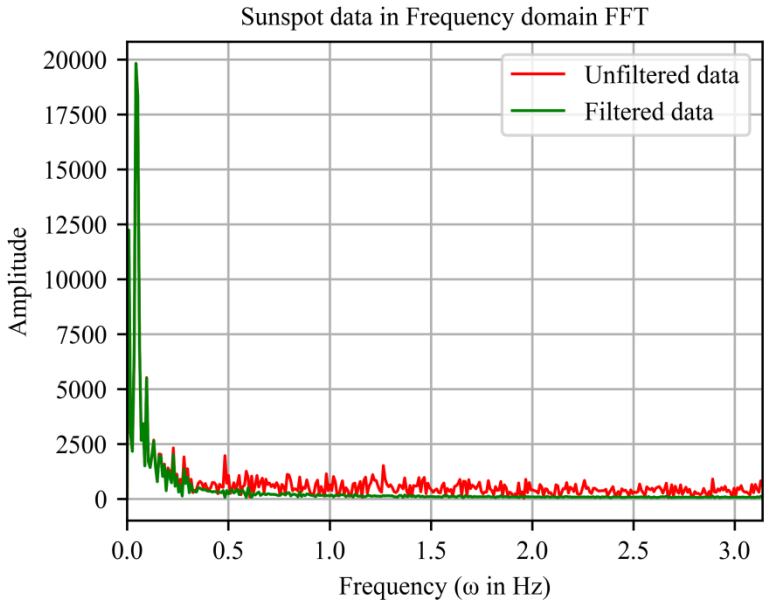

Figure 25: The amplitude spectrum of Sunspot Unfiltered and Filtered data using the FFT method

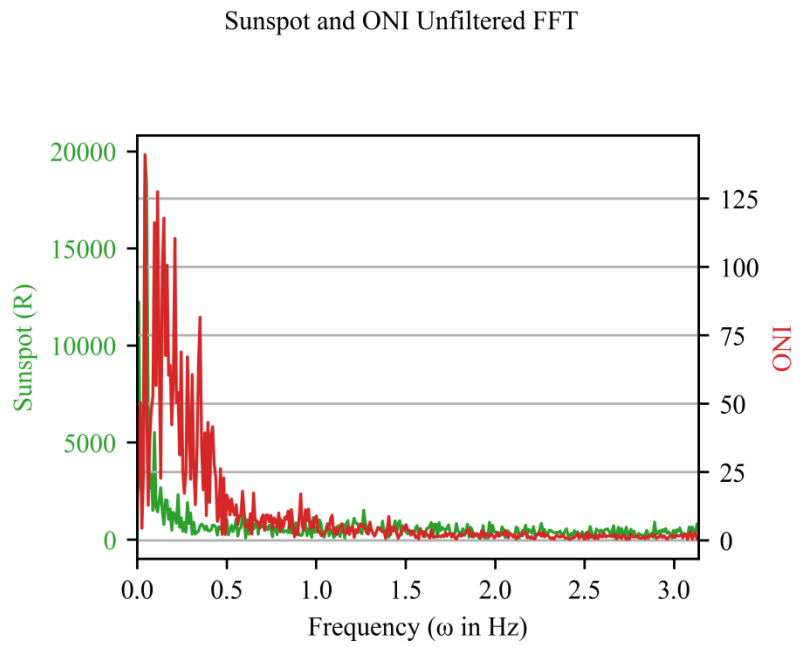

Figure 26: The amplitude spectrum of Sunspot and ONI Unfiltered data using the FFT method

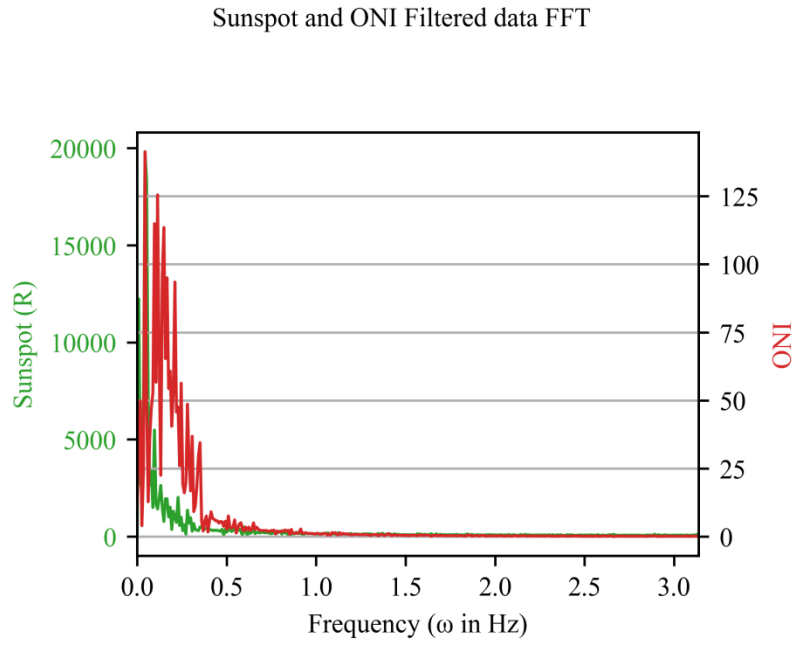

Figure 27: The amplitude spectrum of Sunspot and ONI Filtered data using the FFT method

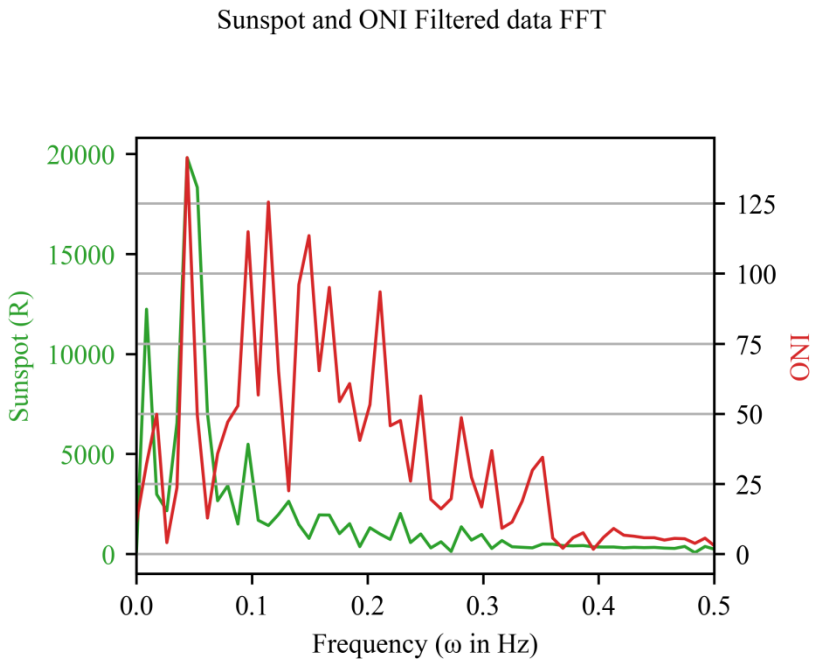

Figure 28: The amplitude spectrum of Sunspot and ONI Filtered data using the FFT method below 0.3 Hz

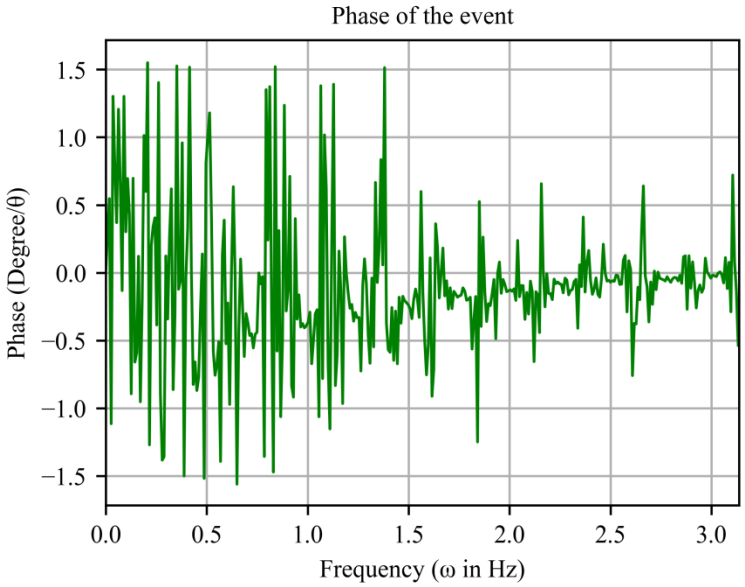

Figure 29: Phase Lag before the regression is calculated